

POLITECNICO DI MILANO

SEDE DI MILANO LEONARDO

Scuola di Ingegneria Industriale e dell'Informazione

Corso di Laurea Magistrale in Ingegneria delle elettrico

Master Degree Thesis

**Solar irradiance attenuation
through high resolution 3D cloud field**



Supervisors:
Prof. Samuele Grillo
Prof. Lorenzo Luini

Candidate:
Ramal Tanveer
Matricola: 851699

Academic year 2015-2016

Abstract

Despite of large potential only a small portion of solar energy reaches at the surface of the earth which is then utilized in power production. It is important to know how this irradiance is effected by the atmosphere especially clouds and how this attenuation affects the working of PV power plant. Thus, the aim of this study is to investigate the attenuation experience by the solar irradiance when passing through the clouds. For this purpose photovoltaic test facility located on roof of the building 14B of POLITECNICO DI MILANO in Via Bonardi 9 is considered. In order to determine solar irradiance reaching the earth surface the estimation of global horizontal irradiance is necessary. It can be calculated through KASTEN clear sky model. Then Global Horizontal Irradiance is split into two components Direct Normal Irradiance and Diffuse Irradiance through DISC model and PEREZ algorithm which is later used to compute irradiation on the PV plane of array. Then, hourly, monthly and yearly PV power production is been calculated through numerical computations introduced by PVWatts. Furthermore to calculate attenuation SMOC(stochastic model of clouds), a methodology to spatially synthesize cloud fields is considered. It provides integrated liquid water content time series. Using this information extinction coefficient is been calculated multiplying the extinction coefficient with the path length of solar rays gives the attenuation due to cloud fields. Lastly CCDF comparison is been made between the actual PV output power, the power calculated through clear sky model and later considering the attenuation factor.

Abstract

Nonostante il grande potenziale, solo una piccola porzione di energia solare raggiunge la superficie della terra che viene poi utilizzata nella produzione di energia elettrica. È importante sapere come questo irraggiamento è attenuato dall'atmosfera, in particolare dalle nuvole, e come questa attenuazione delle radiazioni solari influenzi il funzionamento dei pannelli fotovoltaici. Lo scopo di questo studio è di indagare l'attenuazione dell'irraggiamento solare quando passa attraverso le nuvole. A tal fine viene preso in considerazione l'impianto fotovoltaico di prova situato sul tetto del sito 14B in Via Bonardi 9 del Politecnico di Milano. Per determinare l'irraggiamento solare privo di attenuazione che raggiunge i pannelli solari viene calcolato l'irraggiamento che raggiunge la superficie terrestre utilizzando il modello astronomico "clear sky" KASTEN. A partire da questo dato, viene calcolato, utilizzando il modello DISC e l'algoritmo PEREZ, l'irraggiamento che giunge ai pannelli fotovoltaici e, di conseguenza, la loro produzione. Per il calcolo dell'attenuazione è stato utilizzato il modello SMOC (stochastic model of clouds), che fornisce serie temporali di valori di contenuto liquido delle nubi. I valori forniti dai modelli sono utilizzati per calcolare l'attenuazione dell'irraggiamento solare nel tragitto all'interno dell'atmosfera. I valori di attenuazione sono stati utilizzati per correggere l'irraggiamento fornito dal modello "clear sky" e calcolare nuovamente la produzione dei pannelli fotovoltaici. I valori di potenza prodotta dai pannelli fotovoltaici (dati misurati, dati ottenuti con il modello "clear sky" e dati ottenuti tramite attenuazione del modello "clear sky") sono stati confrontati utilizzando le complementary cumulative distribution functions (ccdf).

Acknowledgments

I would like to thank all those who helped me in drafting this thesis. First of all I would like to thank Prof. Samuele Grillo, for providing me the opportunity to embark this experience, and Prof. Lorenzo Luini for providing detailed knowledge of work and following me throughout the implementation of the software.

I thank Politecnico di Milano for providing me with every means to accomplish my job. Finally, I thank my family who over the years has allowed me to reach this goal, to which this work is dedicated.

Content

Chapter 1

Introduction.....1

Chapter 2 Solar Energy.....3

- Basic Earth Sun Angles.....4
- Relationship between clock time and solar time.....5

Chapter 3 Clear Sky Models.....9

- Extraterrestrial Radiation.....9
- Model to determine the radiation on clear day.....10
- The DISC Model.....12
- DC Power Production.....13

Chapter 4 SMOC Methodology.....15

- Wave Particle Interaction.....18
- Physical Model.....18
- Empirical Model.....18
- Rayleigh Scattering.....19
- MIE Scattering.....19
- Optical Approximation.....19

Chapter 5 Research and Analysis.....21

- PV Test Facility.....21
- Specifications of Monitoring System.....21
- Acquisition System.....21
- MATLAB Simulations.....22
- Prediction of cloud attenuation through SMOC.....24

Chapter 6 Conclusion and Research.....28

References.....29

Appendix.....31

LIST OF FIGURES

Figure 1 The earth revolution around the sun

Figure 2 Position of the earth in relation to the sun's rays at the time of winter solstice

Figure 3 Latitude, hour angle and sun's declination angle

Figure 4 Definition of sun's zenith, altitude and azimuth angles

Figure 5 Model comparison of extraterrestrial radiation

Figure 6 Global Horizontal Irradiance plotted against zenith angle

Figure 7 Vertical profile obtained at a specific value of coefficients

Figure 8 Synthetic map of cloud field

Figure 9 View of test facility

Figure 10 Extraterrestrial radiation reaching the earth atmosphere

Figure 11 Global Horizontal Irradiance vs Time

Figure 12 Direct and Diffuse radiation

Figure 13 Solar zenith angle vs time

Figure 14 Clear sky model and real time comparison

Figure 15 Attenuation map

Figure 16 CCDF comparison 1

Figure 17 CCDF comparison 2

Figure 18 CCDF comparison 3

Figure 19 CCDF comparison 4

CHAPTER 1

INTRODUCTION

Among renewable energy sources, the energy from PV can be considered as most important and endurable source because of profusion of solar energy. Regardless of irregularity of sunlight, solar energy is a renewable, inexhaustible and widely available source of energy. The utilization of solar energy has increased in recent years, Due to the drop in the panel pricings and improvement in solar panel efficiency of photovoltaic has become a major source of energy in recent years. This has remarkably boosted the applications based on photovoltaic usage. PV systems now has been considered as a feasible substitute to grid based energy.

The main direct and indirect derived advantage of solar energy are following: no emission of green house or toxic gases, reclamation of degraded land, reduction of transmission lines from electricity grids, increase of regional/national energy independence, diversification and security of energy supply, acceleration of rural electrification in the developing countries[1].

However, the intermittency of solar energy can cause variability in PV output power. These irregularities come from many factors but mainly from clouds over the sky and it can either increase the power or decrease it i.e. if cloud covers a fraction of sky then the irradiance is shadowed and the rays do not directly strike the panel causing decrease in the power production while if the clouds are not occluding the sun they can reflect the radiation causing an increase in the power production. For the electricity grid the stability is an important phenomena and therefore prediction of attenuation that solar radiation experiences while passing through clouds is important in order to analyze variability in the produced power

The objective of this thesis is to study the effect of cloud field on the solar radiation. The attenuation that is experienced by solar rays when it passes through the clouds is calculated using the integrated liquid water content and micro physical properties of the clouds. Very recently, Luini and Capsoni in [2] have proposed SMOC (stochastic model of clouds), a methodology to synthesize 3D spatially correlated cloud fields. In [2] an accurate model for the vertical profile of the clouds is introduced. In order to calculate irradiance in the absence of cloud clear sky model is implemented which estimates the solar irradiance as a function of time. A 250W Samsung PV panel is used for power calculation for a single day. Once the power for a single day is obtained it can be combined to estimate AC power production for month or even a year.

Once the power from clear sky model is obtained, subtracting the attenuation corresponding to the sun path length will predict actual power production of PV panel. Finally the complementary cumulative distribution function of monthly average is plotted between actual power produced obtained, from the real time data of the site, the power calculated from the clear sky model and power

estimated after attenuation, considering different attenuation factor depending on the site location. The simulations is been performed on the Matlab software.

The structure of the thesis is as follows. Chapter 2 briefly introduces the basic concepts and principles of the solar energy. Chapter 3 discusses about different clear sky models available in literature and a brief comparison between them. Chapter 4 describes the SMOC methodology and different cloud attenuation models. Chapter 5 the whole research, analysis and simulations processes done with regard to the thesis are discussed. Finally the conclusions and future work are discussed in Chapter 6.

CHAPTER 2

SOLAR ENERGY

Solar radiation or light is normally perceived as an electromagnetic wave which travels from point of origin, which is sun to point of observation. The frequency of wave or its wavelength determines the colour of the light. The interpretation of photoelectric effect by Albert Einstein in 1905 gave an insight that solar radiation is just not a wave but also has particle nature. (Hummel 2011) There are various principles which govern the pattern of solar radiation which are discussed in this Chapter.

The sun is the source of most of the energy on the Earth. In order to understand thermal effect of the solar radiation it is important to understand Earth's relationship with the Sun. The earth is nearly spherical with a diameter of about 7,900 miles (12.7×10^3 km). It makes one rotation about its axis every 24 hours and completes a revolution about the sun in a period of approximately 365 1/4 days. The earth revolves around the sun in a nearly circular path, with the sun located slightly off centre of the circle. The earth's mean distance to the sun is about 9.3×10^7 miles (1.5×10^8 km). Since the intensity of solar radiation incident upon the top of the atmosphere varies inversely with the square of the earth-sun distance, the earth receives about seven percent more radiation in January than in July. The earth's axis of rotation is tilted 23.5 degrees with respect to its orbit about the sun. The earth's tilted position is of profound significance. Together with the earth's daily rotation and yearly revolution, it accounts for the distribution of solar radiation over the earth's surface, the changing length of hours of daylight and darkness, and the changing of the seasons.

Figure 1, shows the earth tilted axis at different times of year while figure 2, shows earth tilt with respect to the sun's rays at the time of winter solstice. At winter solstice around 22nd December, the North Pole is away from the sun by 23.5 degrees. At the time of summer solstice around 22nd June, the situation is reversed i.e. the South Pole is tilted 23.5 degrees, while North Pole receives continuous sunlight. At the times of the two equinoxes around 22nd March and 22nd September both poles have equal distant from the sun and the earth's surface has equal hours of day light and darkness

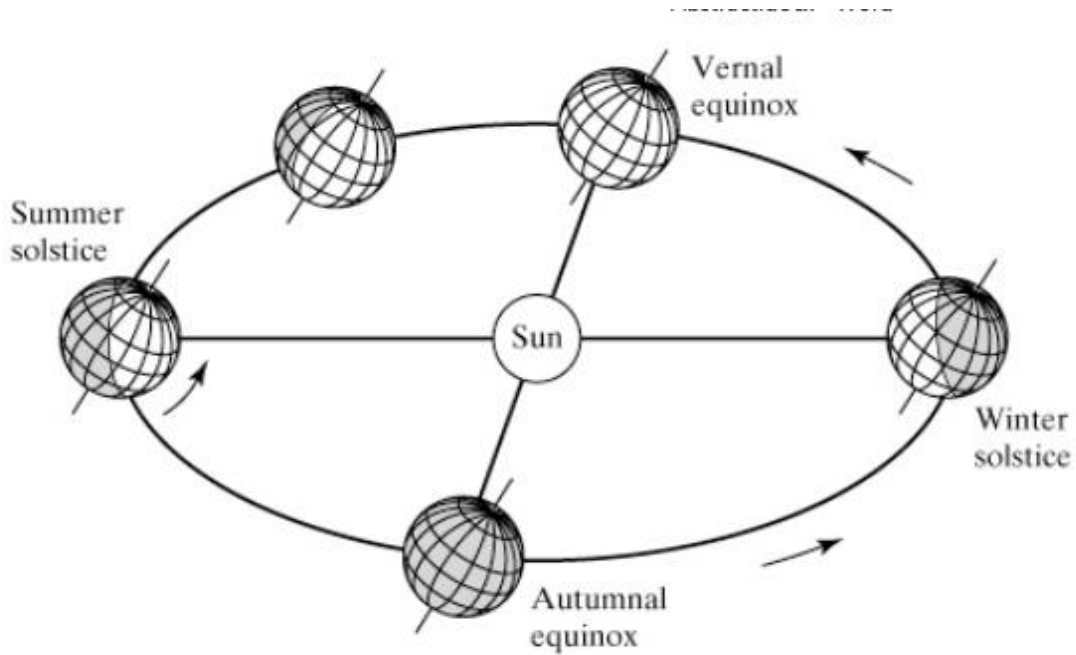


Figure 1: The earth revolution around the sun. The earth's axis of rotation is tilted about 23.5 degrees compared to the plane of earth's orbit around the sun.

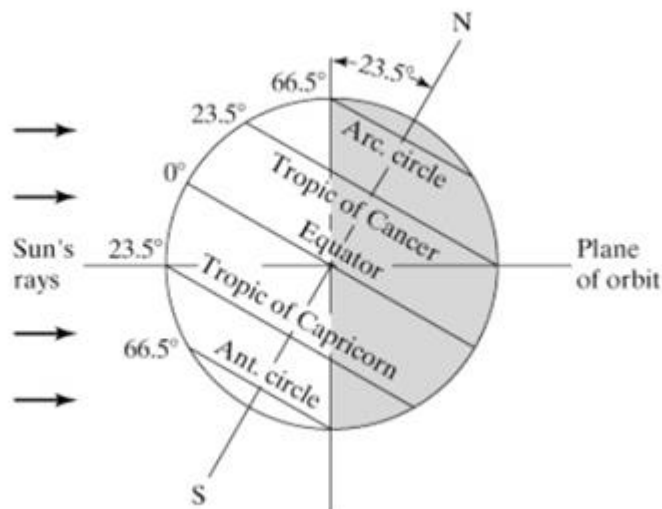


Figure 2: Depicts the position of the earth in relation to the sun's rays at time of winter solstice. The South Pole is tilted towards the sun, while the northern hemisphere is tilted away. This causes summer in South Pole while winter in North Pole.

BASIC EARTH SUN ANGLES:

The position of a point P on the earth's surface with respect to the sun's rays is known at any instant if the latitude, l , and hour angle, h , for the point, and the

sun's declination angle, d , are known. Figure 3 shows these fundamental angles. Point P represents a location on the northern hemisphere.

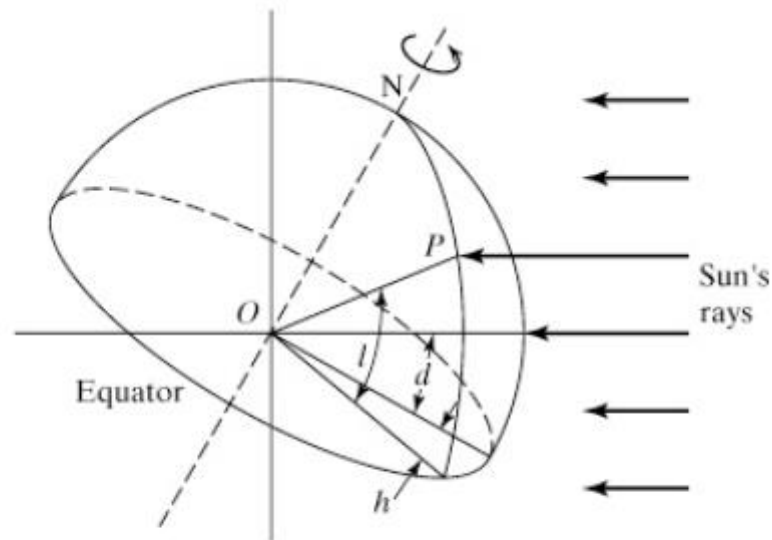


Figure 3: Latitude, hour angle, and sun's declination angle

The latitude, l , is the angular distance of the point P north (or south) of the equator. It is the angle between the line OP and the projection of OP on the equatorial plane. Point O represents the centre of the earth. The calculation of the various solar angles, performed later in this chapter, can be simplified by the adoption of a consistent sign convention. As part of this sign convention, north latitudes are positive and south latitudes are negative.

The hour angle, h , is the angle measured in the earth's equatorial plane between the projection of OP and the projection of a line from the centre of the sun to the centre of the earth. At solar noon, the hour angle is zero. The hour angle expresses the time of day with respect to solar noon. One hour of time is represented by $365/24=15$ degrees of hour angle. As part of the convention, the hour angle is negative before solar noon and positive after solar noon.

The sun's declination angle, d , is the angular distance of a sun's rays north (or south) of the equator. It is the angle between a line extending from the centre of the sun to the centre of the earth and the projection of this line upon the earth's equatorial plane. The declination is positive when the sun's rays are north of the equator and negative when they are south of the equator. At the time of the winter solstice, the sun's rays are 23.5 degrees south of the earth's equator ($d = -23.5^\circ$). At the time of the summer solstice, the sun's rays are 23.5 degrees north of the earth's equator ($d=23.5^\circ$). At the equinoxes, the sun's declination is zero.

The declination angle throughout the year can be well approximated by a sine function [3]:

$$d = 23.45 \sin \left[\frac{360}{365} (284 + n) \right] \quad [\text{degrees}]$$

Where n is the day of the year. The value of n for any day of the month "D" can be determined easily with the aid of Table 1.

<i>Month</i>	<i>n for the Day of the Month, D</i>	<i>Month</i>	<i>n for the Day of the Month, D</i>
January	D	July	181 + D
February	31 + D	August	212 + D
March	59 + D	September	243 + D
April	90 + D	October	273 + D
May	120 + D	November	304 + D
June	151 + D	December	334 + D

Table 1: Variation in "n" throughout the year

RELATIONSHIP BETWEEN CLOCK TIME AND SOLAR TIME:

Solar radiation calculations must be made with respect to the solar time. Time reckoned from midnight at the Greenwich meridian (zero longitude) is known as Greenwich Civil Time or Universal Time. Such time is expressed on an hour scale from zero to 24. Thus, midnight is 0h and noon is 12h. Local Civil Time is reckoned from the precise longitude of the observer. On any particular meridian, Local Civil Time is more advanced at the same instant than on any meridian further west and less advanced than on any meridian further east. The difference amounts to 1/15 hour (4 minutes) of time for each degree difference in longitude. Time as measured by the apparent diurnal motion of the sun is called Apparent Solar Time, Local Solar Time, or Solar Time. Whereas a civil day is precisely 24 hours, a solar day is slightly different due to irregularities of the earth's rotation, obliquity of the earth's orbit and other factors. The difference between Local Solar Time, LST and Local Civil Time, LCT is called the Equation of Time.

The factors described above can be included into a single equation, which relates solar time and clock time:

$$LST = CT + \left(\frac{1}{15}\right)(L_{std} - L_{loc}) + E - DT \quad [\text{hr}]$$

Where:

LST = Local Solar Time [hr]

CT = Clock Time [hr]

L_{std} = Standard Meridian for the local time zone [degrees west]

L_{loc} = Longitude of actual location [degrees west]

E = Equation of Time [hr]

DT = Daylight Savings Time correction (DT = 0 if not on Daylight Savings Time, otherwise DT is equal to the number of hours that the time is advanced for Daylight Savings Time, usually 1hr)

LST must be converted to decimal format from zero to 24. Values of the Equation of Time, E, are calculated by:

$$E = 0.165 \sin 2B - 0.126 \cos B - 0.025 \sin B \quad [\text{hr}]$$

where:
$$B = \frac{360(n - 81)}{364} \quad [\text{degrees}]$$

and n is the day of the year.

Once Local Solar Time is established, the solar hour angle, h can be calculated. By recalling that the hour angle varies at the rate of 15 degrees per hour, that h = 0 at solar noon, and that the sign convention is h < 0 before solar noon, the equation for the hour angle is determined by:

$$h = 15(LST - 12) \quad [\text{degrees}]$$

Besides the latitude, hour angle and sun's declination angle other angles are also useful in solar radiation calculation. These angles are sun's elevation β angle, zenith angle θ_H and azimuth angle φ.

To an observer on earth, sun seems to follow a circular path from horizon to horizon. Figure 4 schematically shows one apparent solar path and defines the sun's zenith, altitude, and azimuth angles. Point P represents the position of the observer, point O is the centre of the earth, and IDN is a vector representing the sun's rays. The zenith angle θ_H is the angle between the sun's rays and local

vertical, i.e. a line perpendicular to the horizontal plane at P. The altitude angle β is the angle in a vertical plane between the sun's rays and the projection of the sun's rays on the horizontal plane. It follows that $\beta + \theta_H = \pi/2 = 90^\circ$. The azimuth angle Φ is the angle in the horizontal plane measured from south to the horizontal projection of the sun's rays.

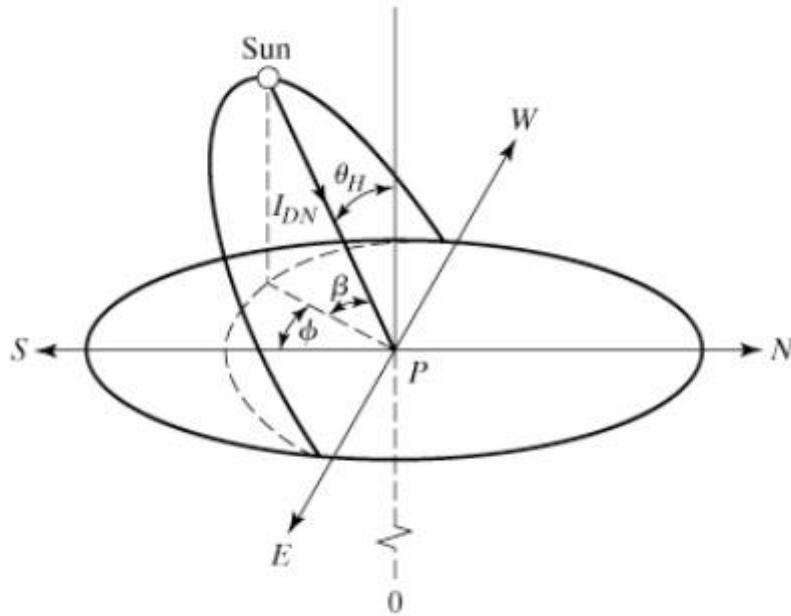


Figure 4: Definition of sun's zenith, altitude, and azimuth angles

Thus the following equations can be derived:

$$\cos \theta_H = \cos l \cos h \cos d + \sin l \sin d$$

Since $\beta = 90 - \theta_H$, [degrees]

$$\sin \beta = \cos l \cos h \cos d + \sin l \sin d$$

The sun's azimuth, ϕ , is given by the relation:

$$\cos \phi = \frac{1}{\cos \beta} (\cos d \sin l \cos h - \sin d \cos l)$$

The above equations allows the calculation of the sun's zenith, altitude and azimuth angles if the declination, hour angle, and latitude are known. Once these angles are known solar radiation can be calculated through different clear sky models.

Chapter 3

CLEAR SKY MODELS

Clear sky models can be helpful in calculation terrestrial radiation under cloudless sky using sun's elevation angle, zenith angle, concentration of aerosols, water vapours and other atmospheric parameters. As we know the solar irradiance is a measure of sunlight intensity (W/m^2), this information can be useful to determine the output of photovoltaic plant at a given day and location.

Forecasting rely on irradiance conversion into a measure of fraction of power reaching the earth for the maximum power reaching that location. Though clouds do not deduct the irradiance by a constant amount (W/m^2), instead they attenuate the sunlight by a certain amount depending on the cloud type. The irregularity in the PV output power generally is parallel to the irregularity of the incidence irradiance.

Even on a clear day, all the extra-terrestrial radiation does not reaches the earth. Normally at noon under clear sky 25% of the extra-terrestrial irradiance from the sun is absorbed and scattered by the atmosphere. In the morning and in evening the attenuation increases due to long path length through the atmosphere. The irradiance coming directly from the sun is called direct normal irradiance or beam radiation. The solar rays that are scattered in all direction through the atmosphere are reflected towards the earth and are called diffuse radiations. These reflection also include reflections from the ground depending on the surface albedo, which in the case of snow can increase. The total solar irradiance on the horizontal surface is known as global horizontal irradiance GHI. The GHI is the sum of direct solar radiation and diffuse solar radiation, this relation can be expressed as:

$$\text{GHI} = \text{Diffuse} + \text{DNI} * \text{COS}(\theta_H)$$

where θ_H is the zenith angle of the sun.

In literature there are many clear sky models are available to measure GHI. Some of them are discussed and compared in this chapter.

Extra-Terrestrial Radiation:

It is the radiation that reaches outer part of the atmosphere and varies slightly throughout the year depending on the day of the year. The extra-terrestrial radiation is calculated by following equation [4]

$$I_o = 1367.7 [1 + 0.033 \cos((2\pi/365)n)]$$

n is the day of the year.

Spencer created a more detailed model [5].

$$I_o = 1366.1 [1.00011 + 0.034221 \cos(x) + 0.00128 \sin(x) - 0.000719 \cos(2x) + 0.000077 \sin(2x)]$$

Another algorithm is been given by NREL’s SOLPOS [6]. The comparison between the 3 models is been plotted in the figure 5, it can be seen that the results are more or less the same.

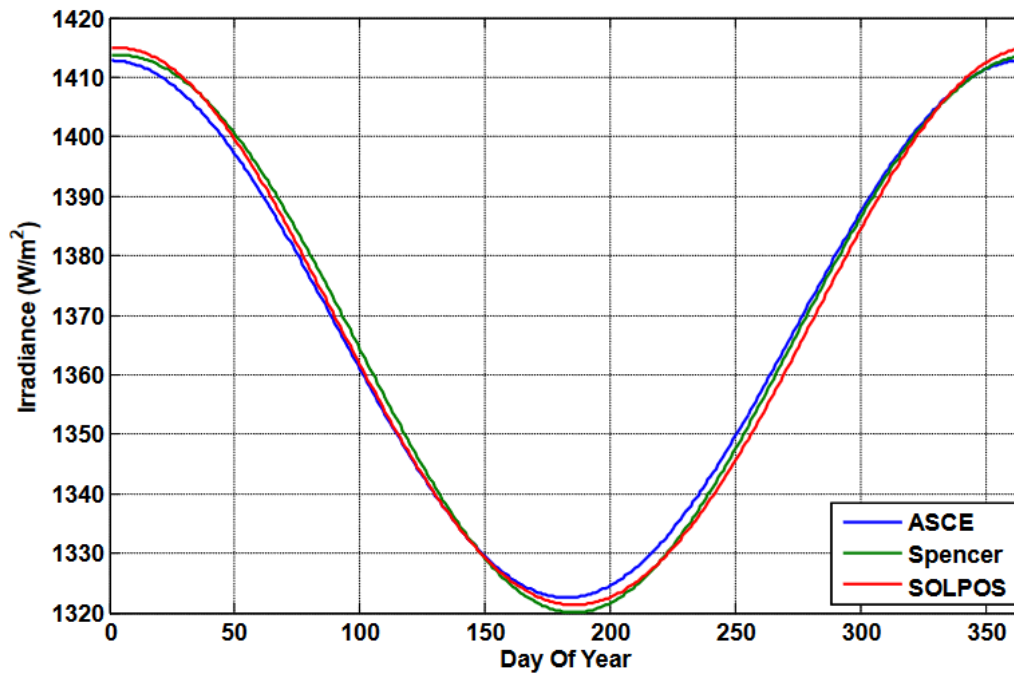


Figure 5: Model comparison

Models to Determine the Radiation on the Clear day

In the following models the reduction in the extra-terrestrial irradiance through the atmosphere is a function of the sun’s zenith angle, larger the zenith angle larger will be the air mass and there will be more interaction of solar radiations with the atmosphere.

Daneshyar-Paltridge-Proctor (DPP) model (1978)[7,8]

$$DNI = 950.2(1 - \exp(-0.075(90^\circ - z)));$$

$$Diffuse = 14.29 + 21.04 \left(\frac{\pi}{2} - z \frac{\pi}{180} \right);$$

$$GHI = DNI \times \cos(z) + Diffuse.$$

Kasten-Czeplak (KC) Model (1980) [9]

$$GHI = 910 \times \cos(z) - 30.$$

Haurwitz Model (1945) [10, 11]

$$GHI = 1098 \times \cos(z) \times \exp\left(\frac{-0.057}{\cos(z)}\right).$$

Berger-Duffie (BD) (1979) [12]

$$GHI = I_0 \times 0.70 \times \cos(z).$$

Adnot–Bourges–Campana–Gicquel (ABCG) Model (1979) [12]

$$GHI = 951.39 \times (\cos(z))^{1.15}.$$

Robledo-Soler (RS) (2000) [17]:

$$GHI = 1159.24 \times (\cos z)^{1.179} \times \exp(-0.0019 \times (90^\circ - z)).$$

As the above mentioned discussed models depends only on the zenith angle of the sun. So, these models are termed as simple clear sky models. Figure 6 depicts the graph plotted between the calculated GHI from these six models vs the zenith angle.

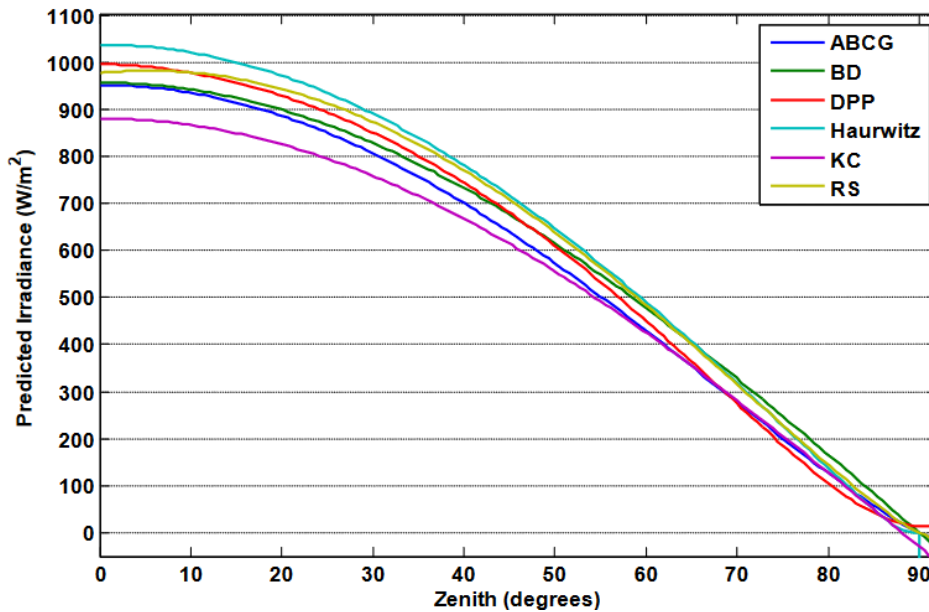


Figure 6

There are also some other models that besides zenith angle also takes in to account some atmospheric parameter such as air pressure, temperature, aerosol content, turbidity and elevation.

One of the clear sky model is Kasten Model [14] which uses linke turbidity, airmass and elevation of the site to evaluate GHI.

Air mass is basically optical path length of the solar rays across the atmosphere. In solar energy it is measured as path length relative to zenith angle i.e.

$$AM = 1/\cos(\theta H)$$

Linke turbidity factor provides the approximation for the scattering and absorption of the solar irradiance in clear sky. It elaborate the optical thickness

of the atmosphere due to aerosol particles with respect to dry and clean atmosphere.

The Kasten model can be expressed as:

$$GHI = 0.84 \times I_0 \times \cos(z) \exp(-0.027) \times AM \times (fh1 + fh2(TL - 1))$$

with $fh1 = \exp(-h/8000)$ and $fh2 = \exp(-h/1250)$

Ineichen and Perez [15] added some correction factors to Kasten model and provide the following expression.

$$GHI = cg1 \times I_0 \times \cos(z) \times \exp(-cg2 \times AM \times (fh1 + fh2(TL - 1))) \times \exp(0.01 \times AM \times 1.8)$$

where $cg1 = 5.09E - 5 \times h + 0.868$ $cg2 = 3.92E - 5 \times h + 0.0387$

As the above discussed model includes different atmospheric parameters therefore it is been chosen for the calculation of solar irradiance for the location under study and the whole set of theoretical data is available.

The DISC MODEL

For the PV panel production computation, it is important to determine the two parameters of global horizontal irradiance i.e. the beam radiation and diffuse radiations. In order to split the GHI into its components the Direction Insolation Simulation Code is implemented. The DISC model was given by Maxwell 1987 [16, 17] it is a quasi-physical model that shows relationship of seasonal variations between effective global horizontal irradiance K_t and direct clearness index K_n . This index is a ratio of measured irradiation at a location relative to the extra-terrestrial irradiance. It is also referred as clearance index and given as

$$K_n = E_n/E_{ext}$$

The relationship between K_n and K_t is a function of air mass, perceptible water vapour and albedo. Maxwell used the parameterization of K_n with respect to K_t . He derived a model equation that produces the change or deviation ΔK_n and ΔK_t from the clear sky transmittance denoted by K_{nc} and K_{tc} deviation from the maximum value is because of atmospheric parameters such as air mass, cloud cover and water vapours. Relationship of ΔK_t and ΔK_n is given as

$$\Delta K_n = K_{nc} - K_n$$

and

$$\Delta K_t = K_{tc} - K_t$$

For the evaluation of maximum direct transmittance value under clear sky, Bird model is used which is given by

$$K_{nc} = 0.866 - 0.122 \times AM + 0.0121AM^2 + 0.000653 \times AM^3 + 0.000014 \times AM^4$$

Then through least square regression method the exponential relationship between ΔK_n and AM is used:

$$\Delta K_n = A + B \times \exp(C \times AM)$$

The cloud cover determines the clearness value of the sky K_t and the three coefficient stated above are dependent on K_t by following relation

If $K_t < 0.60$ (cloudy conditions)

$$A = 0.512 - 1.56 \times K_t + 2.286 \times K_t^2 - 2.222 \times K_t^3$$

$$B = 0.370 + 0.962 \times K_t$$

$$C = -0.280 + 0.932 \times K_t - 2.048 \times K_t^2$$

If $K_t \geq 0.60$ (clear sky conditions)

$$A = -5.743 + 21.77 \times K_t - 27.49 \times K_t^2 + 11.56 \times K_t^3$$

$$B = 41.40 - 118.5 \times K_t + 66.05 \times K_t^2 + 31.90 \times K_t^3$$

$$C = -47.01 + 184.2 \times K_t - 222.0 \times K_t^2 + 73.81 \times K_t^3$$

So, the direct beam transmittance K_n can be calculated if we have maximum value of beam transmittance K_{nc} and deviation from its maximum value ΔK_n

i.e.
$$K_n = K_{nc} - \Delta K_n$$

Then multiplying his direct beam transmittance with the extra-terrestrial irradiance gives the direct normal radiation.

$$DNI = I_o \times K_n$$

Once the direct normal radiation is computed, the diffuse radiation can be calculated through geometrical manipulation of the following equation

$$GHI = DNI \times \cos(\theta_H) + Diffuse$$

Finally we can then determine the ground reflected radiations. The ground reflectance varies with the surface albedo and its value depends on the ground cover. In case of brown grass the reflectance is 0.2, while if the ground cover is soil, the reflectance is 0.1 while the ground with the snow has a reflectance value of 0.87 [18].

DC Power Production

To calculate the power generated by a PV system a module is used suggested in [19]. To compute the DC power from the plane of array the following formulations are used

$$P_{dc} = \frac{I_{tr}}{1000} \cdot P_{dco} (1 + \gamma(T_{cell} - T_{ref}))$$

where

P_{dc} = Power of PV System

P_{dco} = Name-plate DC rating

I_{tr} = Transmitted I_{POA}

γ = temperature coefficient equals $-0.5 \text{ \%}/^{\circ}\text{C}$

T_{cell} = Cell Temperature

T_{ref} = Reference cell temperature equals 25°C .

Once the DC power is obtained, considering the inverter efficiency and module efficiency. DC power can be converted into AC output power for a single day further more monthly average can also be calculated.

CHAPTER 4

SMOC METHODOLOGY

In the related literature numerous prediction models are available for cloud attenuation. A physical globally applicable model was proposed by Dissanayake et al [20]. The attenuation was calculated according to the classified properties of four cloud types and their probability of occurrences. The properties include the average liquid water content, vertical and horizontal extent of the cloud. Though Dissanayake model is global and hence proved to predict cloud attenuation at different sites with good accuracy, its applicability depends on the knowledge of cloud cover, which is not easy to retrieve globally.

Another contribution to cloud attenuation phenomena was proposed by Salonen and Uppala [21] and it is also adopted by the ITU-R recommendation [22]. This model takes into account the microphysical properties of clouds and vertical liquid water, as well as temperature profiles to calculate attenuation for slant path.

Recently, Luini and Capsoni in [2] have proposed SMOC (Stochastic Model of Clouds), a methodology to synthesize 3D spatially correlated cloud fields. The most important notion of SMOC is that, by introducing appropriate statistical features of the integrated liquid water content on the basis of real cloud fields, observed by remote sensing instruments it is possible to synthesize realistic cloud fields globally. Specifically, through SMOC, knowing the mean value of the cloud liquid water content over the targeted area it is possible, to synthesize the cloud field.

The high resolution 3D cloud field is synthesize by the following method

Through E_w derive the μ_p and σ_p according to the expressions

$$\mu_p(E_w) = -5.61 E_w^{-0.076} + 4.69$$

$$\sigma_p(E_w) = 1.03 E_w^{-0.029} - 0.81$$

μ_p and σ_p defines the conditional probability lognormal function of the standard deviation of the cloud water content w .

$$p(S_w|E_w) = \frac{1}{S_w \sigma_p \sqrt{2\pi}} \exp\left[-\frac{(\ln S_w - \mu_p)^2}{2\sigma_p^2}\right]$$

From the obtained lognormal distribution extract S_w with a random draw.

Generate a random Gaussian field $g(x,y)$ with the spatial correlation P_G

$$P_G(d) = 0.35 e^{-d/7.8} + 0.65 e^{-d/225.3}$$

Calculate μ_{LN} and σ_{LN} of the lognormal distribution characterizing the cloud map to be generated

$$\text{(for } W > 0 \text{ mm): } \begin{cases} \mu_{LN} = \ln\left[\frac{1}{f_w^{1.5}} \frac{E_w^2}{\sqrt{E_w^2 + S_w^2}}\right] \\ \sigma_{LN} = \sqrt{\ln\left[f_w \left(\frac{S_w^2}{E_w^2} + 1\right)\right]} \end{cases}$$

While E_w and S_w in the above equation are taken from the NWP database, the μ_{LN} and σ_{LN} are the mean and standard deviation values of a random variable whose values is zero with the probability of $1-f_w$ the fraction of map where is no cloud and it is obtained from the lognormal distribution with the probability of f_w .

Turn the Gaussian field $g(x,y)$ into a log normal field $C(x,y)$ using the following transformation

$$C(x,y) = \exp\left\{ \begin{array}{l} \mu_{LN} + \sqrt{2}\sigma_{LN}\text{erfc}^{-1} \\ \left[\frac{1}{f_w} \text{erfc}\left(\frac{g(x,y)}{\sqrt{2}}\right) \right] \end{array} \right\}$$

Randomly extract the cloud base height h_o from the PDF i.e.

$$p(h_0) = \frac{1}{\sigma} t(h_0)^{\xi+1} e^{-t(h_0)} \quad \text{with} \quad t(x) = \begin{cases} \left[1 + \left(\frac{x-\mu}{\sigma} \right)^\xi \right]^{-1/\xi} & \xi \neq 0 \\ e^{-(x-\mu)/\sigma} & \xi = 0 \end{cases}$$

where $\xi = 0.484$, $\sigma = 0.582$, and $\mu = 0.987$.

For each pixel in the map, calculate a and b, these two parameters determine the vertical profile of the liquid water content $w(h)$

$$a = 4.27 e^{-4.93(W+0.06)} + 54.12 e^{-61.25(W+0.06)} + 1.71$$

$$b = 3.17 a^{-3.04} + 0.074$$

Once a and b are known the vertical profile can be generated by the following expression

$$\tilde{w}(h) = \begin{cases} \frac{W}{b^a \Gamma(a)} (h-h_0)^{a-1} e^{-(h-h_0)/b} & \text{for } h \geq h_0 \\ 0 & \text{for } h < h_0 \end{cases}$$

Figure 7 depicts the sample vertical profiles obtained at a specific value of a and b [2].

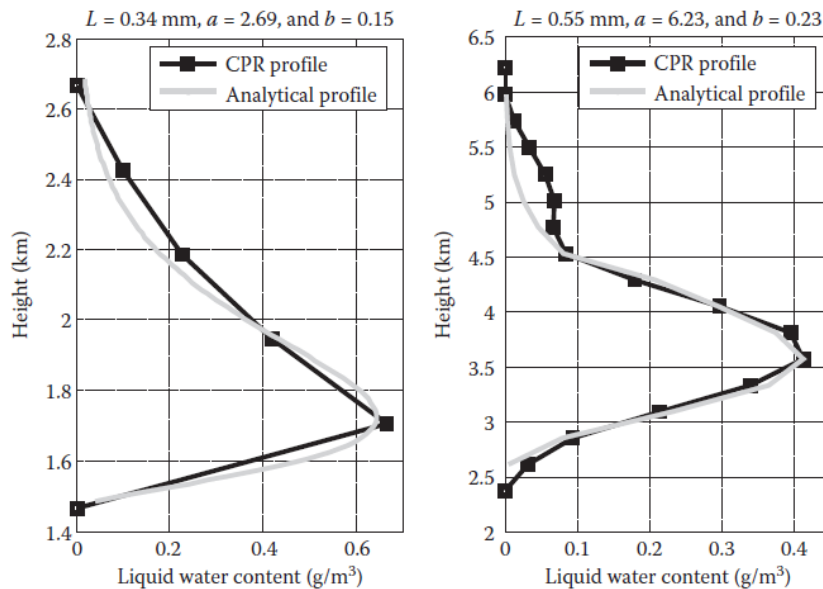


Figure 7

Figure 8 is the sample map that can be obtained through SMOC.

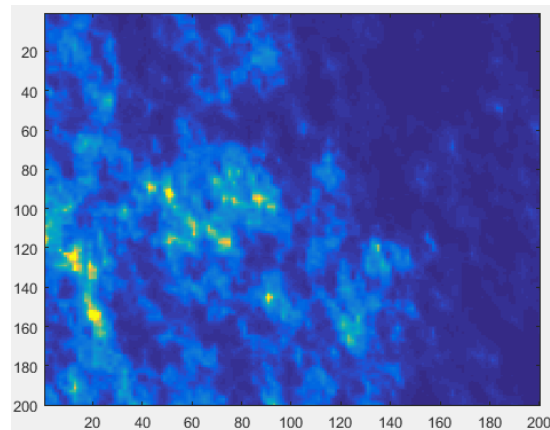


Figure 8 Synthetic map of cloud field

With the analysis of different of different profiles it is noted that the peak value of liquid water content is closer to the cloud base and with increasing height the profiles gradually drops to zero.

A key point for predicting attenuation through cloud fields is the development of the vertical profile of the liquid water content with in cloud, which can be obtained through SMOC.

Wave- Particle Interaction

Wave attenuation through the atmospheric parameters is usually calculated based on two approaches

Physical models: primarily based at the microphysical and electromagnetic properties of individual particles. First, the interaction among the incoming radiation and a single particle is taken into consideration. The single contributions are eventually added up to find the amount of energy subtracted from the incoming wave. The task becomes much more complicated when multiple scattering is taken into account. Physical models use additional information such as the data such as particle size distribution and hence provide results with good accuracy.

Empirical models: depend upon empirical relationships linking wave attenuation to the liquid water content in clouds. The empirical models depends on local data, they are valid locally with the compromise of accuracy.

When an electromagnetic wave hits a particle, a part of the wave is absorbed by the particle and released as heat, while the another part is scattered in various directions. In short the electromagnetic wave loses an amount of its energy.

When the wave strikes a particle, by knowing the intensity of the wave and the extinction coefficient associated to the particle, the attenuation can be calculated. The extinction coefficient depends on various factors such as wavelength, polarization of the incident, wave, particle size, composition and shape.

The Earth's atmosphere is composed of gases. These gases and other constituent particles in atmosphere e.g. pollutants cause the scattering of incoming solar radiation.

There are basically three types of scattering according to which different extinction coefficients can be defined.

Mie Scattering

Mie scattering is used to define scattering of the incident white light by way of particles of massive diameter within the surroundings. The bigger particles in surroundings scatter all the components of radiations in a same way. The clouds in the sky appears to be white to the observer as a cease end of the incoming radiations and it also produces white light by scattering through the fog. Additionally Mie scattering takes area specifically at lower layers of the atmosphere where the large particles are in majority. The elements in atmosphere which causes Mie scattering are clouds, hall, aerosols and rain particles.

The other two approximations are as follows:

Rayleigh Scattering

This type of scattering occurs when particles are much smaller than the incoming radiation wavelength. Rayleigh in the 19th century derived a cross section for small size particles compared to the wavelength (Sneep, Ubachs 2005) the equation is as follows:

$$\sigma = \frac{32\pi^3}{3\lambda^4 N^2} (n - 1)^2,$$

Where σ is the cross section, N is the molecules density and λ is the wavelength of the wave and n is the refractive index of the particle. The blue sky effect is the most common effect caused by Rayleigh scattering. The wavelength of blue end is larger so it gets scattered while the red end of the spectrum has shorter wave length so it not effected. (Young 1981) the scattering intensity was also calculated by the following equation

$$I = I_0 \left(\frac{8\pi^4 N \alpha^2}{\lambda^4 R^2} \right) (1 + \cos^2 \theta),$$

Where, α is the polarizability
 R is the distance from the scatter
 Θ is the angle of scattering
 I_0 is the initial intensity

Optical Approximation

If the size of the particle is much larger than the wavelength of the impinging wave, the geometrical optics can be used to solve the scattering problem. In this case there are two possibilities either the light ray gets reflected or refracted by the striking the particle, about (10 – 20%) portion of light gets absorbed by the particle and remain 80 % get scattered. On the other hand light ray can get diffracted. This light results in certain distribution of intensity.

According to (Van de Hulst 1957), if the particle is far greater than the incident ray, the extinction cross section becomes twice as the geometric cross section of the particles i.e.

$$\sigma_{ext} = 2 \pi r^2$$

As a result the extinction coefficient can be expressed as [23].

$$\beta_{ext} = 6.51 \times 10^3 \frac{w}{\rho r_e} \quad (\text{dB/km})$$

Where w is the liquid water content expressed in g/m^3
 ρ is the density of water expressed in g/cm^3
 r_e is the effective radius of the particle

The above equation is applicable cloud droplets in the visible range. For larger wavelengths i.e. in IR regions different expressions for the extinction coefficient are used.

For the prediction of attenuation due to clouds, a model for size distribution is generally considered. Four parameter modified gamma function $n(r)$ is often adopted, which is flexible and widely used for cloud droplets:

$$n(r) = ar^\alpha e^{-br^\gamma}$$

where r is the particle radius and a , b , γ and α are four independent parameters.

The attenuation induced by the cloud particles can be calculated as:

$$A = \int_{l_0}^{l_{max}} \beta_{ext}(\lambda) dl \quad (\text{DB})$$

where β_{ext} is the specific attenuation. Figure 9 depicts the sample specific attenuation time series.

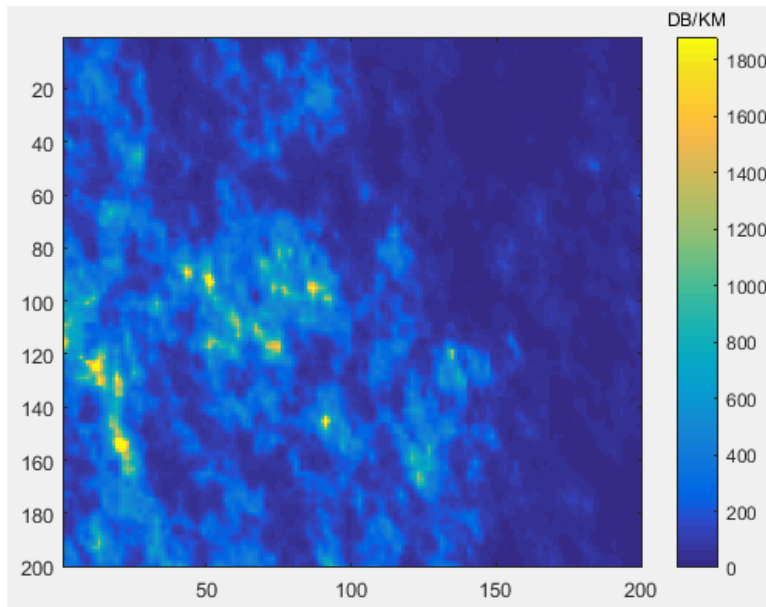


Figure 9-Specific attenuation map

Chapter 5

Research and Analysis

The aim of the Chapter is to study attenuation of the solar radiation and its matlab simulation.

PV test Facility

The photovoltaic modules are installed at the POLITECNICO DI MILANO experimental station in Milan, covering the building 14B in Via Bonardi 9. The monitoring station is equipped with climatic detection equipment and support structures that allow the angle inclination of tested modules to vary. The experimental station is equipped with 16 micro-inverters that allow continuous data acquisition of photovoltaic module performance. The stations used in this monitoring are 13.

Specifications of Monitoring Stations

Below are the features of the monitoring station, the instrumentation available for data surveys and the technologies installed during the monitoring period.

The building 14B rooftop has been equipped with metallic structures that allow the installation and incline of photovoltaic modules with different inclination angles. For the monitoring conducted at this stage, the modules were fastened by means of clamps to the supporting structures so that the surface of the grid is oriented with an azimuth angle equals to zero and angle of inclination is 30° .



Figure 10- View from the west and east of the modules installed at the test facility of the Politecnico di Milano.

Acquisition System

Data output from the modules is captured by 300W micro Aurora inverters that allow to connect to the network and to monitor each module individually. The inverters have the ability to track the maximum power point (MPPT) for each single module minimizing efficiency losses in any type of condition. The peak

efficiency is 96.5%. The appendix shows the technical datasheet of the micro inverter used.

Though the test report of PV monitoring station analyzed 4 modules with different technologies, but for this study, only Samsung module (LPC250SM-06) is considered because of its positive power output tolerance it avoids the power loss and highly efficient. The datasheet of the module is added in the Appendix.

MATLAB Simulations

The Perez clear sky model described in chapter 2 is been implemented in Matlab. Figure 11 depicts the extraterrestrial radiation reaching the earth atmosphere at 15th of May.

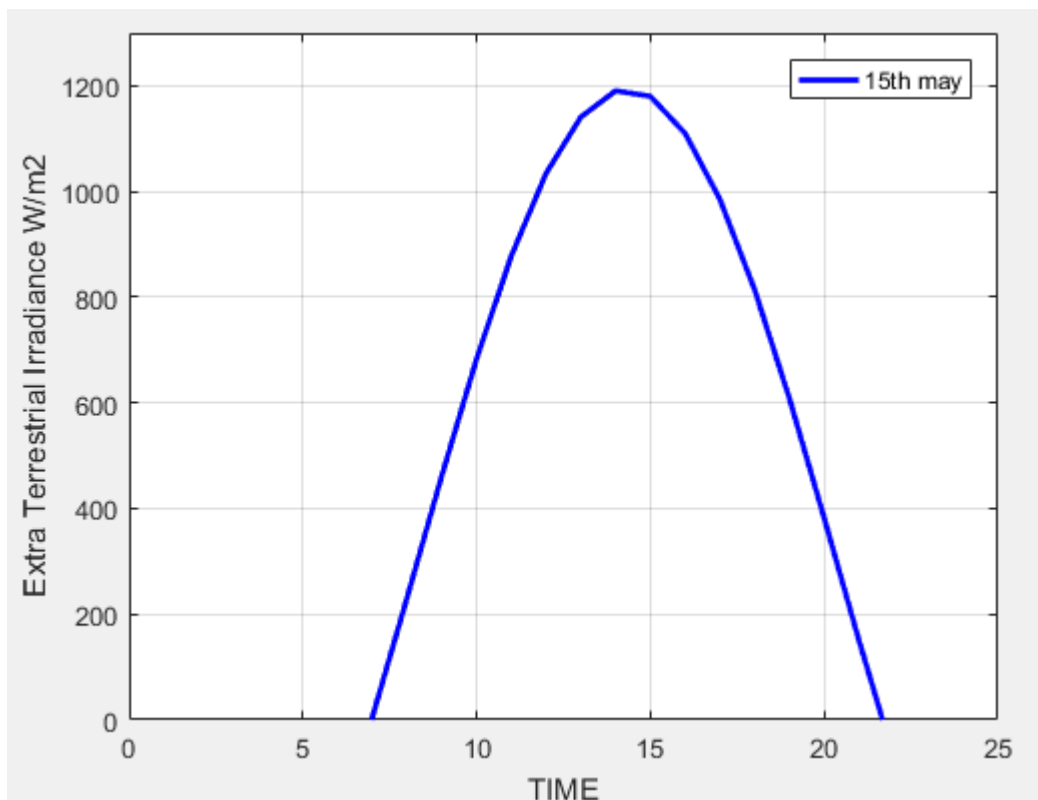


Figure 11- Extra-terrestrial radiation reaching the earth atmosphere.

Global horizontal Irradiance obtained through the clear sky model for 15th of May is shown in figure 12.

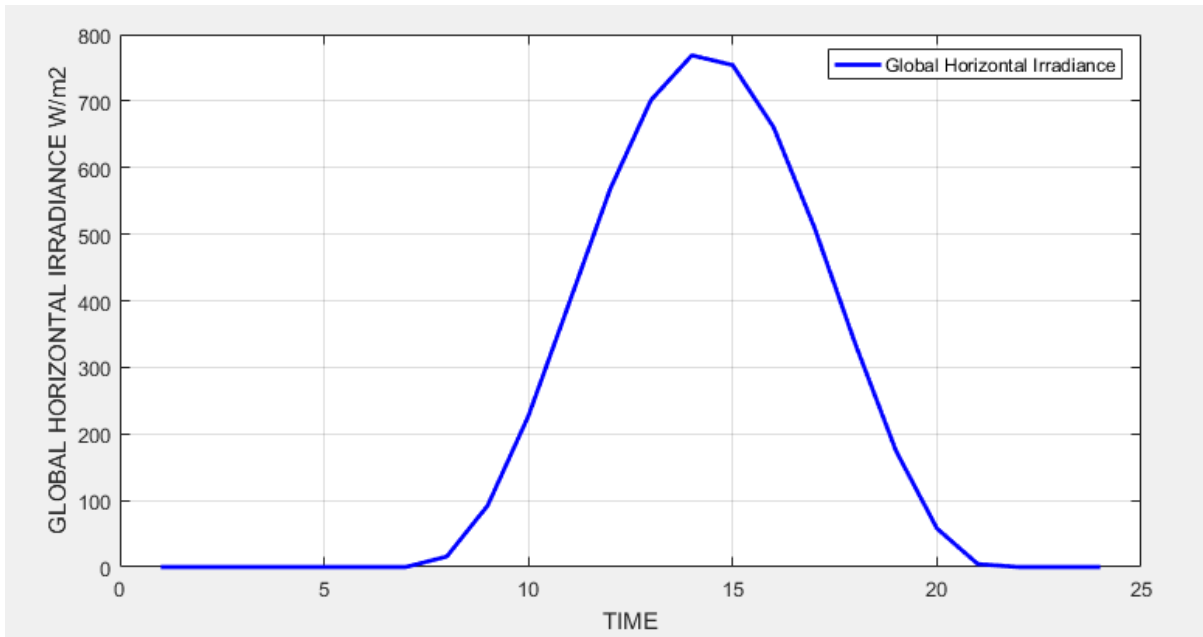


Figure 12- Global Horizontal irradiance

As already described in the chapter 2 the global horizontal irradiance has two components the diffuse radiation and the direct normal radiation. These two components have been extracted through DISC model and are plotted for 15th of May (166 day of the year) in the figure 13. As the direct normal irradiance depends on zenith angle of the sun the figure14 depicts the zenith angle plot for 15th of May.

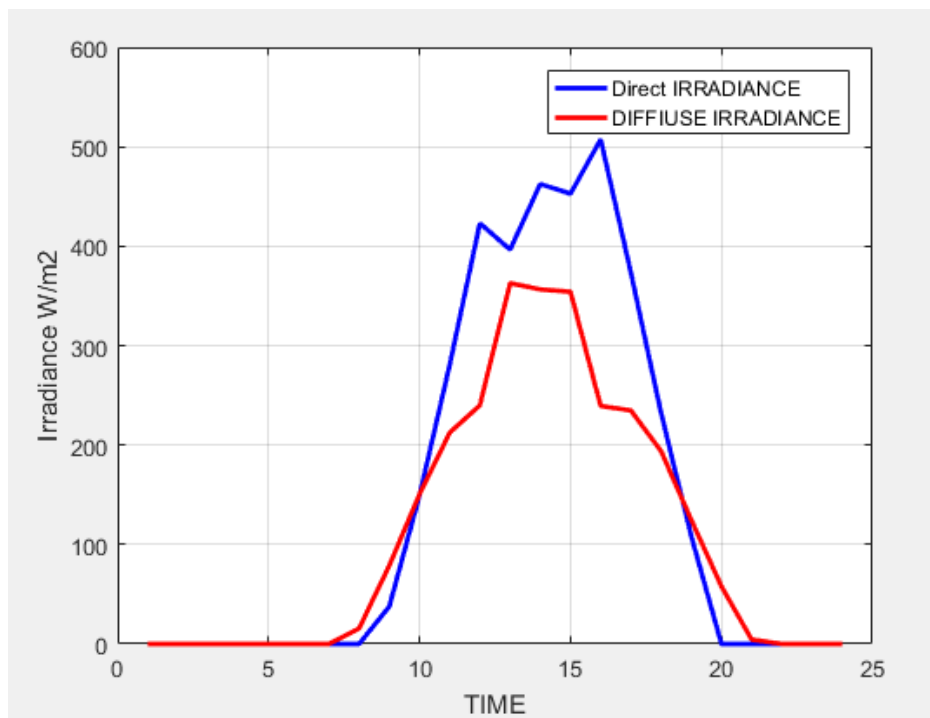


Figure 13-Direct and Diffuse irradiance

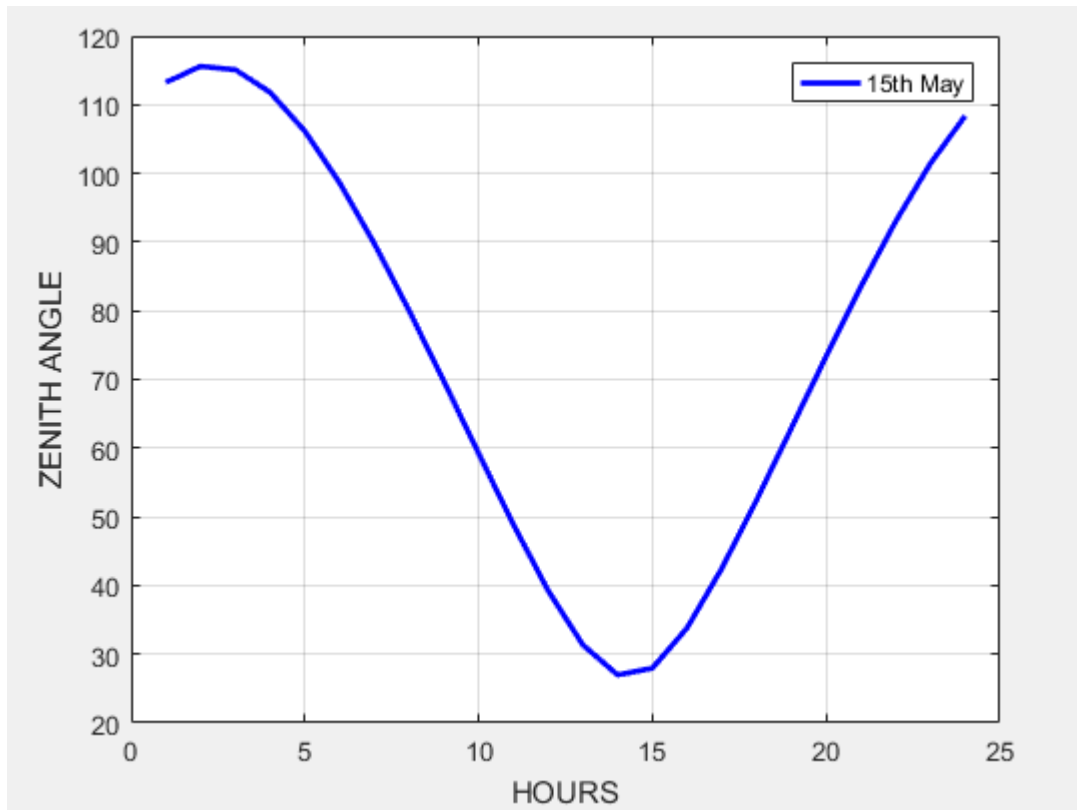


Figure 14- Solar Zenith angle of 15th may

Once the direct and diffuse radiation is obtained on the plane of array of PV module then the calculations suggested by PV WATT are been performed to compute AC output power [19], DC output power is calculated by taking into account parameters from Samsung datasheet.

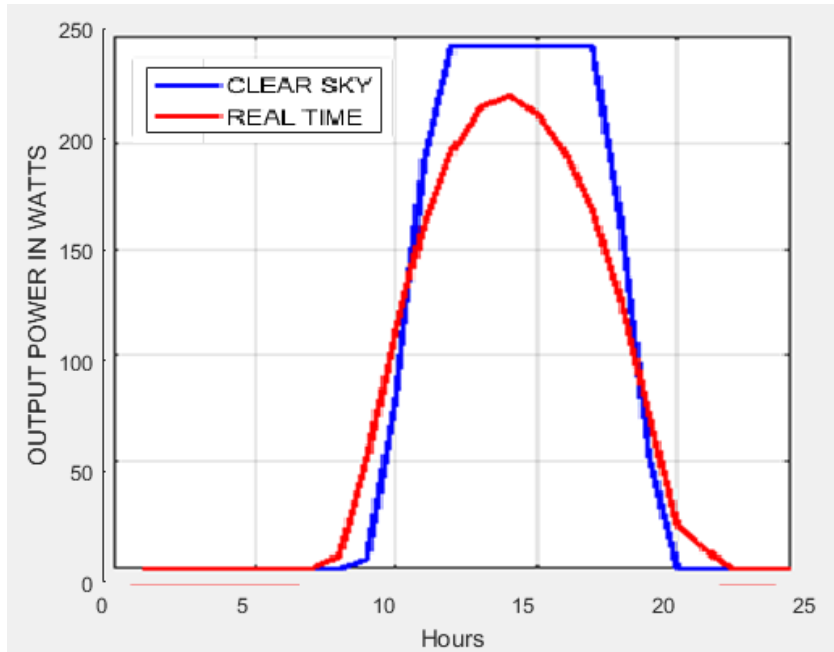


Figure 15- Clear sky model and real time comparison

In order to plot CCDF comparison between the clear sky, attenuated and real time data the hourly computations of clear sky model was interpolated into 15 minutes intervals and the hours considered for the analysis are 0am, 6am, 12 pm and 18 pm. Each hour contains 5 samples with ± 15 minute i.e. for 0 am the extracted samples are -30 am -15am 0am +15am +30am. For each sample hour the synthesize cloud map is been generated through SMOC. So basically for a single day 4 sample maps are available. The attenuation was calculated for each map, as there are 5 samples per hour, but attenuation calculated for a single hour is considered same for all of its 5 samples, assuming that the cloud cover does not change frequently.

Once the attenuation for every sample is obtained subtracting it from the clear sky irradiance samples we get the loss in the solar irradiance and then corresponding AC power can be computed for the attenuated irradiance.

In the following figures a CCDF comparison is been made for the production data of 3 years i.e. 2014, 2015 and 2016.

CCDF COMPARISON FOR YEAR 2014

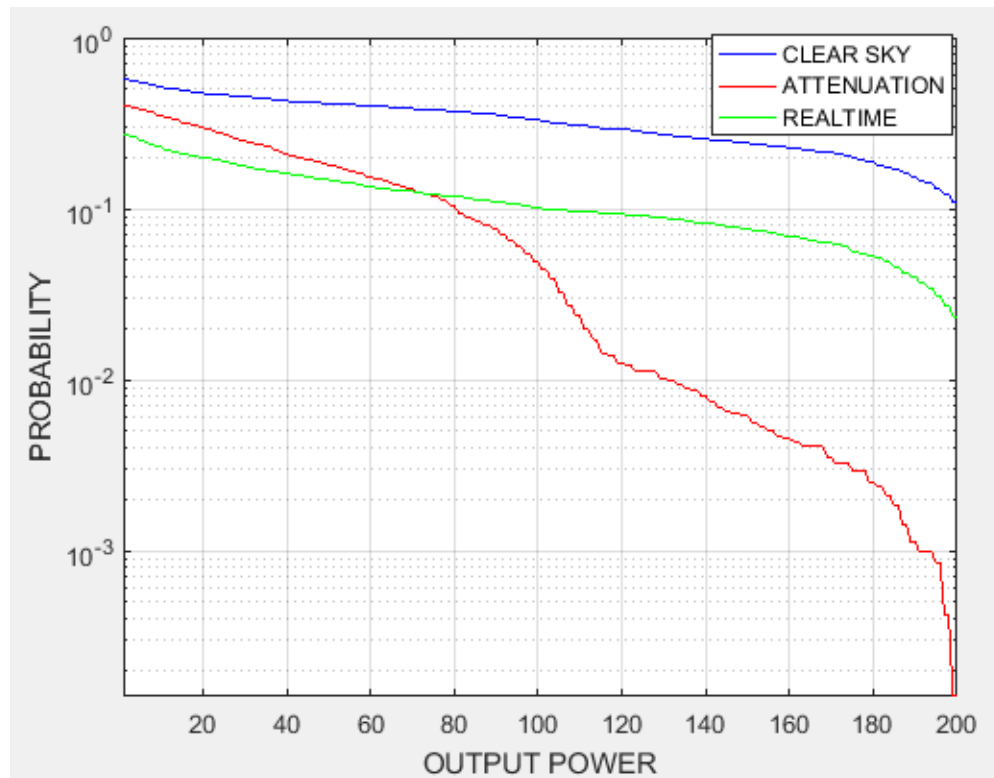


Figure 16 shows the CCDF comparison between the real time data, Clear sky model and attenuation model.

CCDF COMPARISON FOR YEAR 2015

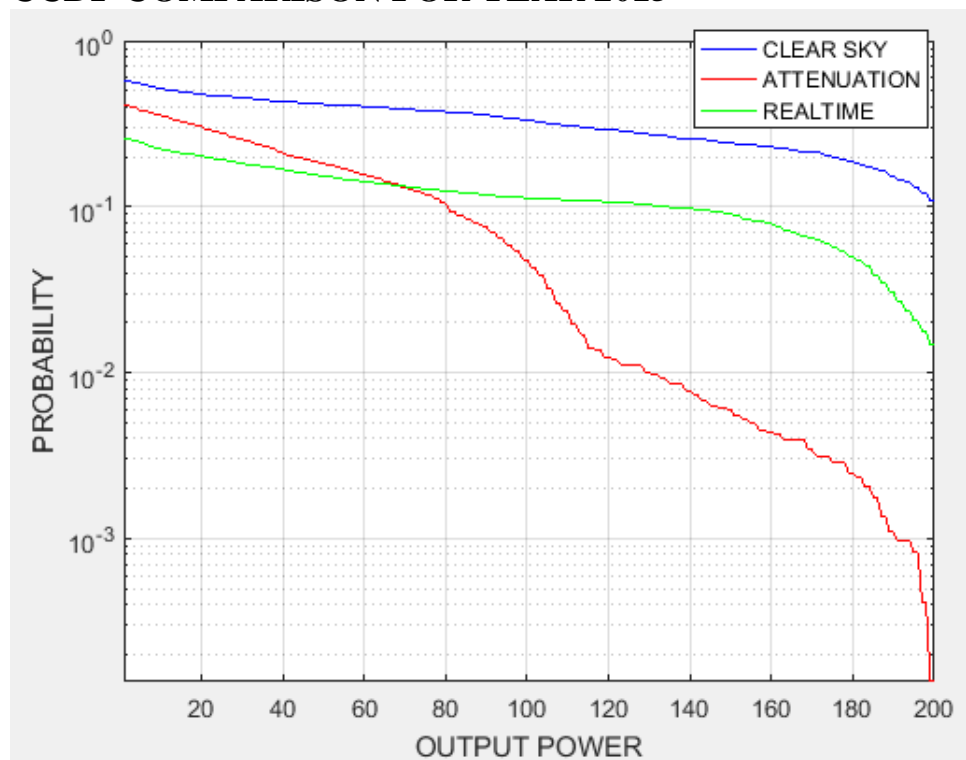


Figure 17 shows the CCDF comparison between the real time data, Clear sky model and attenuation model for year 2015.

CCDF COMPARISON FOR YEAR 2016

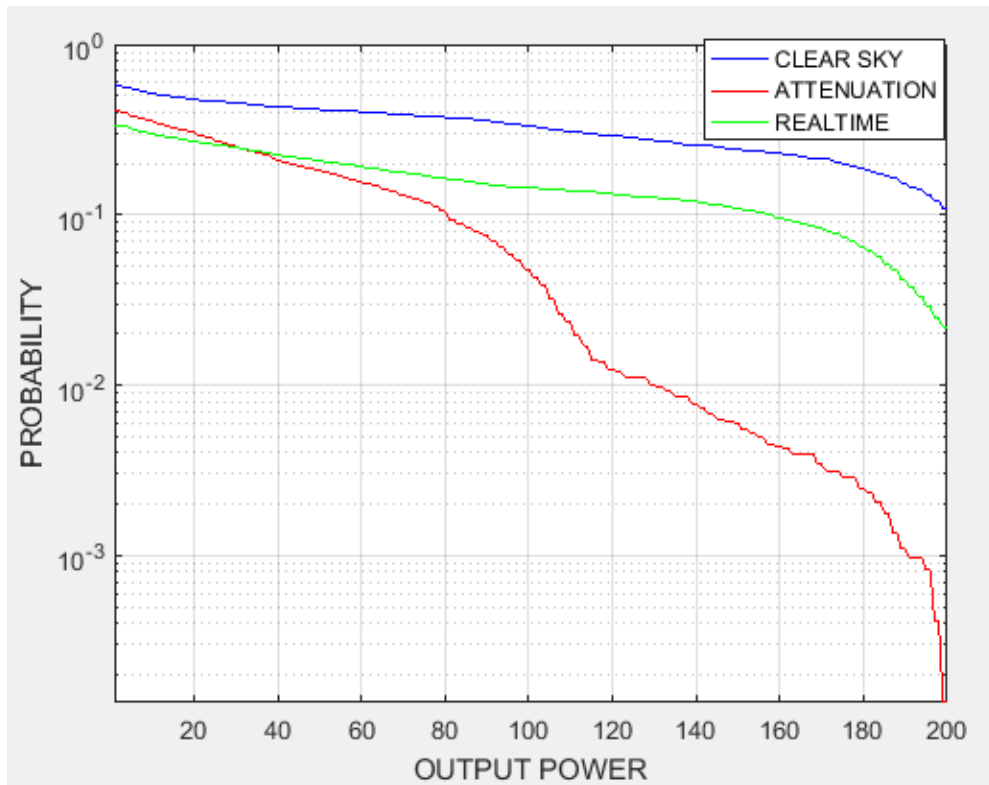


Figure 18 shows the CCDF comparison between the real time data, Clear sky model and attenuation model for year 2016.

CCDF COMPARISON FOR 3 YEARS COMBINED

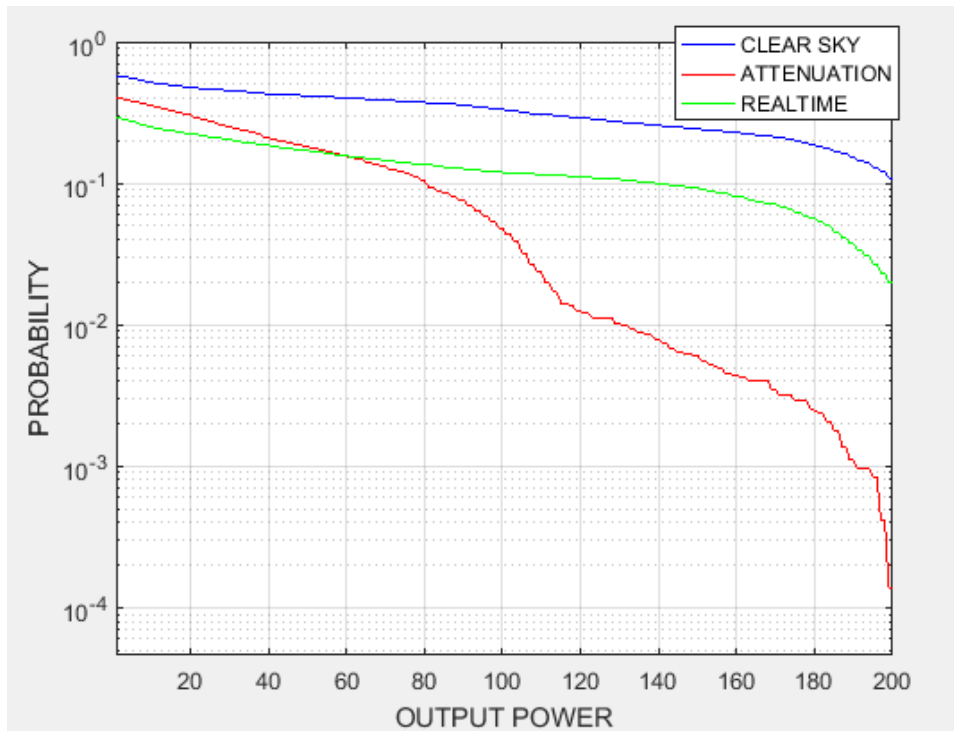


Figure 19 shows the CCDF comparison between the real time data, Clear sky model and attenuation model for 3 years combined.

According to the comparisons made in the figure 19 it can be stated that even for the same ground location there is different probability of cloud coverage. We see that the transmission of radiation rapidly decreases with the increasing thickness of the cloud cover for the heavy cloud coverage, the power that the PV module will be producing is about 50W so in this case a simple beam from the sun to the panels is enough to obtain accurate results because here it is assumed that the sky will be fully overcasted and direct irradiance component will be totally blocked by the clouds while the fraction of diffuse irradiance reaching the PV panel will produce the small amount of power as predicted. But for the power range greater than 50W the results are not satisfying because the cloud coverage is lighter i.e. when the clouds are not fully covering the sky then in this case more complex approach is required because the actual intensity of solar radiations is variable under the partly cloudy sky. In this case to predict power after attenuation is challenging because to estimate global horizontal irradiance, two sets of computations needs to be combined i.e. one with clear sky and other considering the clouds, later the diffuse and direct components has to be extracted from these sets of calculations in short more refined approach is needed in order to get accurate results.

CHAPTER 6

Conclusion and Future Research Work

In this study a methodology for the calculation of cloud attenuation to the solar radiations is presented. The calculations specifically relies on the liquid water content obtained through stochastic model of clouds. The methodology explained takes input the latitude, height of the site from the ground, its azimuth angle and predicts the attenuation for single as well as for the multiple slant paths of solar rays. The 3D representation of the cloud field has proved to be accurate methodology to predict the interaction between the solar irradiance and cloud particles and the synthetic cloud fields has helped to calculate extinction coefficient which further leads to obtain the attenuation through the clouds. The results obtained can further be improved by including the effect of haze and correcting the estimation of linke turbidity. Also an improved version of Perez model can be implemented, though it is complex but it can help for better estimation of extinction coefficient which then involves detailed cloud microphysics which will leads in more accurate prediction of cloud attenuation.

REFERENCES

- [1] Vorster F.J., van Dyk E.E., Leitch A.W.R., "Investigation on the I-V characteristics of a high concentration, photovoltaic array", Conference Record of the Twenty-Ninth IEEE Photovoltaic Specialists Conference, pp.1604-1607, 2002.
- [2] L. Luini, C. Capsoni, "Modeling High-Resolution 3-D Cloud Fields for Earth-Space Communication Systems," *IEEE Transactions on Antennas And Propagation*, vol.62, no.10, pp.5190, 5199, Oct. 2014.
- [3] *Appendix D: Solar Radiation*, University of Minnesota, Minneapolis, MN.
- [4] R. G. Allen, Environmental, and E. Water Resources institute. Task Committee on Standardization of Reference, The ASCE standardized reference evapotranspiration equation. Reston, Va.: American Society of Civil Engineers, 2005.
- [5] J. W. Spencer, "Fourier series representation of the sun," *Search*, vol. 2, p. 172, 1971.
- [6] NREL. (February 2000). SOLPOS: Solar Position and Intensity. Available: <http://rredc.nrel.gov/solar/codesandalgorithms/solpos/>
- [7] M. Daneshyar, "Solar radiation statistics for Iran," *Solar Energy*, vol.21, pp. 345-349, 1978.
- [8] G. W. Paltridge and D. Proctor, "Monthly mean solar radiation statistics for Australia," *Solar Energy*, vol. 18, pp. 235-243, 1976.
- [9] F. Kasten and G. Czeplak, "Solar and terrestrial radiation dependent on the amount and type of cloud," *Solar Energy*, vol. 24, pp. 177-189, 1980.
- [10] B. Haurwitz, "Insolation in Relation to Cloudiness and Cloud Density," *Journal of Meteorology*, vol. 2, pp. 154-166, 1945.

- [11] B. Haurwitz, "Insolation in Relation to Cloud Type," *Journal of Meteorology*, vol. 3, pp.123-124, 1946.
- [12] V. Badescu, "Verification of some very simple clear and cloudy sky models to evaluate global solar irradiance," *Solar Energy*, vol. 61, pp. 251-264, Oct 1997.
- [13] L. Robledo and A. Soler, "Luminous efficacy of global solar radiation for clear skies," *Energy Conversion and Management*, vol. 41, pp. 1769-1779, 2000.
- [14] F. Kasten, "A Simple Parameterization of the Pyrheliometric Formula for Determining the Linke Turbidity Factor," *Meteorologische Rundschau*, vol. 33, pp. 124-127, 1980.
- [15] P. Ineichen and R. Perez, "A new air mass independent formulation for the Linke turbidity coefficient," *Solar Energy*, vol. 73, pp. 151-157, 2002.
- [16] Maxwell, Eugene L. *A quasi-physical model for converting hourly global horizontal to direct normal insolation*. No. SERI/TR-215-3087. Solar Energy Research Inst., Golden, CO (USA), 1987.
- [17] Nicholas A. Engerer, "simulating photovoltaic array performance using radiation observed from the Oklahoma mesonet", M.S Thesis, Department of Meteorology, University of Oklahoma, Norman, Oklahoma, 2011.
- [18] *Appendix D: Solar Radiation*, University of Minnesota, Minneapolis, MN.
- [19] Dobos, Aron P. "PV Watts Version 1 Technical Reference." National Renewable Energy Laboratory, Report Number TP-6A20-60272 (2013).
- [20] A. Dissanayake, J. Allnutt, and F. Haidara, "Cloud attenuation Modelling for SHF and EHF applications," *Int. J. Satell. Commun.*, vol. 19, pp. 335–345, 2001.
- [21] E. Salonen and S. Uppala, "New prediction method of cloud attenuation," *Electron. Lett.* , vol. 27, no. 12, pp. 1106–1108, Jun. 1991.
- [22] ITU-R Recommendation P.840-6, "Attenuation due to clouds and fog." Geneva, Switzerland, 2013.

[23] L. Luini, R. Nebuloni, “Impact of Clouds from Ka Band to Optical Frequencies”, Chapter 8, Radio Wave Propagation and Channel Modeling for Earth–Space Systems Taylor and Francis Group, CRC Press, 2016.

APPENDIX

Aurora Micro-0.3-I Inverter Data Sheet

MICRO-0.25-I MICRO-0.3-I

CARATTERISTICHE GENERALI MODELLI DA ESTERNO

Il nuovo micro-inverter Aurora da 250 & 300 Watt offre qualcosa di completamente innovativo ai clienti Power-One: la possibilità di collegare alla rete singolarmente ciascun modulo di uno specifico impianto è un'alternativa ai tradizionali inverter di stringa Aurora, grazie ai quali Power-One è diventata famosa.

I micro-inverter presentano specifici vantaggi rispetto agli inverter di stringa. Permettono di controllare singolarmente l'uscita dei pannelli e offrono la funzione di inseguimento del punto di massima potenza (MPPT) per ogni singolo modulo minimizzando le perdite di efficienza in ogni tipo di condizione.



Caratteristiche

- Convertitore di potenza senza condensatori elettrolitici per aumentare ulteriormente la durata di vita e l'affidabilità a lungo termine del prodotto
- Costruzione da esterno per uso in qualsiasi condizione ambientale
- Produzione di energia potenziata grazie all'algoritmo MPPT, che opera a livello di ciascun pannello fotovoltaico in qualsiasi condizione di luminosità
- L'isolamento in alta frequenza consente l'adattamento a ogni applicazione che richiede il collegamento a terra del polo positivo in ingresso
- Efficienza di picco 96.5%
- Facile da installare grazie all'implementazione di un impianto dotato di hub proprietario di comunicazione wireless
- Ridotta sensibilità al guasto. In caso di malfunzionamento di un elemento, verrà persa soltanto l'energia prodotta da quel particolare modulo fotovoltaico
- Ridotti costi operativi e di manutenzione degli impianti

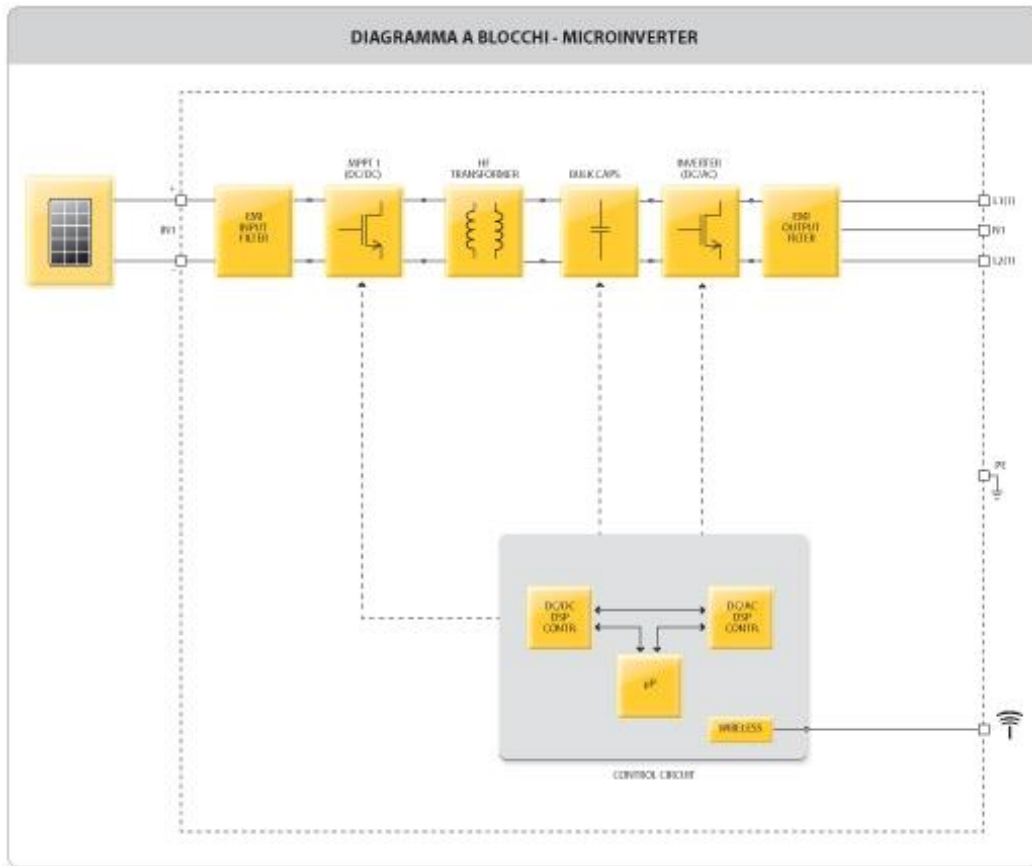
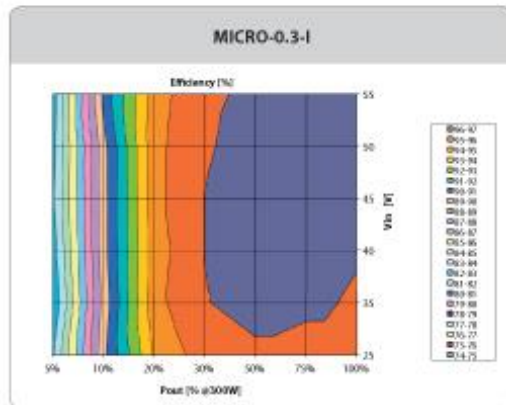
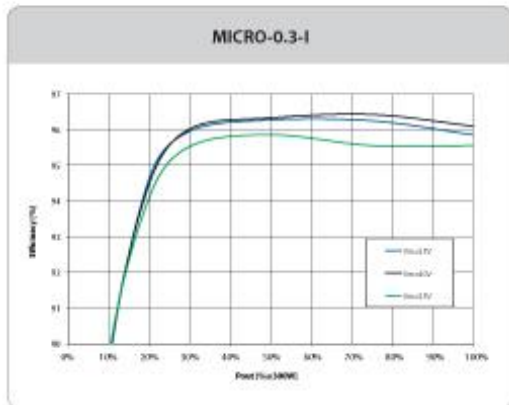


Diagramma a Blocchi e Curve di Efficienza



PARAMETRI	MICRO-0.25-I-OUTD	MICRO-0.3-I-OUTD
Ingresso		
Massima Potenza DC in Ingresso (P_{DCmax})	265 Wp	320 Wp
Intervallo Operativo di Tensione DC in Ingresso ($V_{Min}...V_{Max}$)	12...60 V	12...60 V
Intervallo MPPT di Tensione DC ($V_{MPPTmin}...V_{MPPTmax}$)	25...60 V	30...60 V
Massima Tensione Assoluta DC in Ingresso (V_{MaxAbs})	65 V	65 V
Massima Corrente DC in Ingresso (I_{DCmax})	10.5 A	10.5 A
Numero di Coppie di Collegamento DC in Ingresso per ogni MPPT	1	1
Tipo di Connessione DC	Connettore PV Tool Free WM / MC 4	Connettore PV Tool Free WM / MC 4
Tensione di Attivazione DC di Ingresso (V_{Min})	25V	25V
Uscita		
Tipo di Connessione AC alla Rete	Monofase	Monofase
Potenza Nominale AC di Uscita (P_{AC})	250 W	300 W
Tensione Nominale AC di Uscita (V_{AC})	230 V	230 V
Intervallo di Tensione AC di Uscita ($V_{ACmin}...V_{ACmax}$)	180...264 V ⁽¹⁾	180...264 V ⁽¹⁾
Massima Corrente AC di Uscita (I_{ACmax})	1.3 A	1.5 A
Frequenza Nominale di Uscita (f_r)	50 Hz	50 Hz
Intervallo di Frequenza di Uscita ($f_{min}...f_{max}$)	47...53 Hz ⁽²⁾	47...53 Hz ⁽²⁾
Fattore di Potenza Nominale ($\cos\phi_{I_{AC}}$)	> 0.95	> 0.95
Numero Massimo di Unità per stringa	17	17
Protezioni di Uscita		
Protezione Anti-Islanding	In accordo alla normativa locale	In accordo alla normativa locale
Protezione da Sovratensione di Uscita - Varistore	Si	Si
Prestazioni Operative		
Efficienza Massima (η_{max})	96.5%	96.5%
Efficienza Pesata (η_{LDC}/η_{LIC})	95.4% / -	95.5% / -
Consumo in Stand-by	< 50mW	< 50mW
Comunicazione		
Sistema di Monitoraggio (PC/Data logger)	Wireless	Wireless
Monitoraggio Remoto	Wireless	Wireless
Ambientali		
Temperatura Ambiente	-40...+75°C / -40...167°F con Derating sopra 65°C (149°F)	-40...+75°C / -40...167°F con Derating sopra 65°C (149°F)
Umidità Relativa	0...100 % con condensa	0...100 % con condensa
Emissioni Acustiche	< 30 db(A) @ 1 m	< 30 db(A) @ 1 m
Massima Altitudine Operativa senza Derating	2000 m / 6560 ft	2000 m / 6560 ft
Fisici		
Grado di Protezione Ambientale	IP 65	IP 65
Sistema di Raffreddamento	Naturale	Naturale
Dimensioni (H x L x P)	266mm x 246mm x 35mm / 10.5" x 9.7" x 1.37"	266mm x 246mm x 35mm / 10.5" x 9.7" x 1.37"
Peso	< 1.65 kg / 3.5 lb	< 1.65 kg / 3.5 lb
Sicurezza		
Livello di Isolamento	Trasformatore Alta Frequenza	Trasformatore Alta Frequenza
Certificazioni	CE	CE
Norme EMC e di Sicurezza	EN61000-6-2, EN61000-6-3, EN61000-3-11, EN61000-3-12, EN 50178	EN61000-6-2, EN61000-6-3, EN61000-3-11, EN61000-3-12, EN 50178
Norme di Connessione alla Rete	Enel Guideline (CEI 0-21 + Allegato A70 Terna) ⁽³⁾ , VDE 0126-1-1, VDE-AR-N 4105 ⁽⁴⁾ , G83/1, RD1663, AS 4777	Enel Guideline (CEI 0-21 + Allegato A70 Terna) ⁽³⁾ , VDE 0126-1-1, VDE-AR-N 4105 ⁽⁴⁾ , G83/1, RD1663, AS 4777
Modelli Disponibili		
Standard	MICRO-0.25-I-OUTD-230	MICRO-0.3-I-OUTD-230

1. L'intervallo di tensione di uscita può variare in funzione della norma di connessione alla rete, valida nel Paese di installazione.
2. L'intervallo di frequenza di uscita può variare in funzione della norma di connessione alla rete, valida nel Paese di installazione.
3. Dalle date di applicabilità, limitatamente ad impianti >2kW.
4. Limitatamente ad impianti <3,68kW.

Nota: Le caratteristiche non specificatamente menzionate nel presente data sheet non sono incluse nel prodotto.

Module Profile SAMSUNG LPC250SM-06 (MSG 1.2)

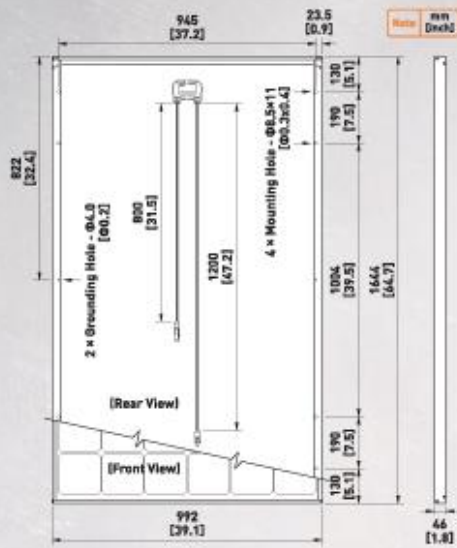


SAMSUNG DELIVERS HIGH EFFICIENCY

SP + series
PV-MBA1AG244 / PV-MBA1AG247 / PV-MBA1AG250



- **High Efficiency**
Samsung solar modules deliver high efficiency, requiring less installation space and lower BOS costs.
- **Positive Power Output Tolerance**
Samsung solar modules and cells avoid any power loss due to its positive output tolerance (0 ~ +2%) and narrow sorting range.
- **Superior Durability**
Samsung solar modules are certified to withstand high pressure: wind loads (2,400Pa), snow loads (5,400Pa).
- **Strict Quality Test**
Samsung solar modules are best-in-class thanks to our quality assurance system following international standard IEC 61215.
- **Eco-Friendly**
Following PV Cycle program, Samsung solar modules will be collected and recycled at the end of their useful life.



Physical characteristics		
Cells per module	60	
Cell type	Mono-crystalline silicon	
Module dimensions	1644x992x46mm (64.7x39.1x1.8 inches)	
Module weight	20.2kg (44.5 lbs)	
Front Glass	Low iron tempered glass	
Junction box	Connector type	MC4
	IP grade	IP65
	Output cables	(-) 800mm, (+) 1200mm (-) 31.5 inches, (+) 47.2 inches

Temperature coefficients	
NOCT	45 ± 2°C
TC Isc	0.033%/K
TC Voc	-0.327%/K
TC Pmax	-0.444%/K

(NOCT : Nominal Operating Cell Temperature)

Packing configuration	
Container	40'HC
Pieces per pallet	20
Pallets per container	26

Dealer information box

PV-MBA1AG244 | PV-MBA1AG247 | PV-MBA1AG250

Measured at STC : Irradiance 1000W/m ² , AM 1.5, and cell temperature 25°C				
Maximum power	P _{max} (Wp)	244	247	250
Maximum power voltage	V _{mp} (V)	30.3	30.4	30.6
Maximum power current	I _{mp} (A)	8.06	8.13	8.17
Open circuit voltage	V _{oc} (V)	37.3	37.5	37.8
Short circuit current	I _{sc} (A)	8.55	8.59	8.62
Module efficiency		14.96%	15.15%	15.33%

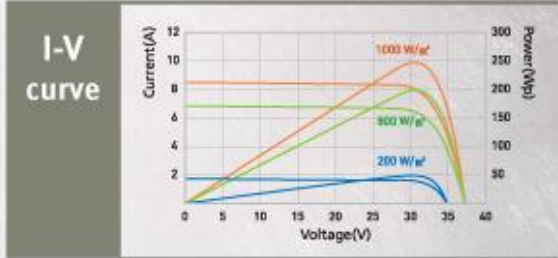
Measured at NOCT : Irradiance 800W/m ² , ambient temperature 20°C, wind speed 1m/s				
Maximum power	P _{max} (Wp)	176	179	182
Maximum power voltage	V _{mp} (V)	27.9	28.1	28.4
Maximum power current	I _{mp} (A)	6.52	6.56	6.65
Open circuit voltage	V _{oc} (V)	33.9	34.2	34.5
Short circuit current	I _{sc} (A)	6.79	6.89	6.97

★ Power output may vary by 0% / +2% and other electrical parameters by ±3%

System integration parameters	
Maximum system voltage (IEC)	1,000V
Maximum system voltage (UL)	600V
Maximum series fuse rating	15A
Limiting reverse current	15A

Safety ratings & Warranties	
Fire Safety Classification	Class C
Certifications	IEC 61215, IEC 61730, UL 1703
Warranty	5 years limited product warranty
Performance guarantee	10 years limited warranty of 90% power output
	25 years limited warranty of 80% power output

Qualification test	
Temp cycling range	-40°C to 85°C for 200cycles
Damp heat test	85°C and 85% relative humidity for 1000hr
Front load test (Snow)	5400Pa
Rear static load test (Wind)	2400Pa
Hailstone impact test	25mm hail at 23m/s from 1m distance



★ All data subject to change without prior notice.

SAMSUNG SDI CO., LTD.
 San# 24 Nongseo-Dong, Giheung-Gu, Yongin-City, Gyeonggi-Do, Korea 446-711
<http://www.samsungsdi.com> | Latest update : August 2011
 Copyright 2011 SAMSUNG SDI



Programming and Coding

```
clc
clear
SUMIpoa=0;
Month=zeros(1,12);
PDC=zeros(1,12);
PAC=zeros(1,12);
Year=zeros(1,12);
ATTE=zeros(1,12);
dni=zeros(24,1);
array=zeros(200,200);
array1=zeros(200,200);
out = load('Clouds_41.mat');
val=(squeeze(out.Cvol(10,:,:)));
for da=1:365;
declination_angle=23.45*sind(360*(284+da)/365);
del=declination_angle*pi/180;
LSTM=15*(2);
N=(360/365)*(da-81);
EoT=9.87*sind(2*N)-7.53*cosd(N)-1.5*sind(N);
TC=4*(9.191383-30)+EoT;
if da<= 31
    TL=3.5;
    Q=28;
elseif da >=32 && da <=59
    TL=4.1;
    Q=36;
elseif da >=60 && da <=90
    TL=3.9;
    Q=44;
elseif da >=91 && da <=120
    TL=4.2;
    Q=52;
elseif da >=121 && da <=151
    TL=5;
    Q=60;
elseif da >=152 && da <=181
    TL=5.3;
    Q=68;
elseif da >=182 && da <=212
    TL=4.9;
    Q=60;
```

```

elseif da >=213 && da <=243
    TL=4.2;
    Q=52;
elseif da >=244 && da <=273
    TL=4;
    Q=44;
elseif da >=274 && da <=304
    TL=3.9;
    Q=36;
elseif da >=305 && da <=334
    TL=3.4;
    Q=28;
elseif da >=335 && da <=365
    TL=3.2;
    Q=28;
end
for y=1:200
for x=1:200
    w=val(y,x);
    beta=(6510)*(w/10);
    Att=beta*(1/sind(Q));
    array1(y,x)=Att;
end
end

HR=da*24;
HR1=HR-23;
h=121;
I0=1367;
a=30;
I=I0*(1+0.033*cosd((360*da)/365));
h=121;
ho=1;
for LT=1:24;
    lt=LT-1;
    LST=lt+TC/60;
    Hour_Angle=15*(LST-12);
    Elevation=asind(sind(declination_angle)*sind(45.46421)+cosd(declination_angle)*cosd(45.46421)*cosd(Hour_Angle));
    phi=90-Elevation;
    Az=acosd((sind(declination_angle)*sind(45.46421)-cosd(declination_angle)*sind(45.46421)*cosd(Hour_Angle))/cosd(Elevation));
    Azi=real(Az);

```



```

if(Hour_Angle<=0)
azimuth=Azi;
elseif(Hour_Angle>0)
azimuth=360-Azi;
end
dni(LT,1)=Elevation;
AM=1/cosd(phi);
f1=exp(-h/8000);
f2=exp(-h/1250);
GHI=0.84*I0*cosd(phi)*exp(-0.027*AM*(f1+f2*(TL-1))); %Kasten Model%
GHI(phi>87 | GHI<1) = 0;
DayAngle = 360.*(da-1)/365;
re = 1.00011 + 0.034221 .* cosd(DayAngle) + (0.00128) .*
sind(DayAngle)+0.000719.*cosd(2.*DayAngle) + (7.7E-
5).*sind(2.*DayAngle);
Io = re.*1370;
Ioh= Io.*cosd(phi);
Ztemp = phi;
Ztemp(phi>87)=87;
AM1=(cosd(phi)+0.15*((93.885-Ztemp).^(-1.253))).^-1;
Kt=GHI/Ioh;
if(Kt<=0.60)
A = 0.512 - 1.56.*Kt +2.286.*(Kt.^2) - 2.222.*(Kt.^3);
B= 0.37 + 0.962.*Kt;
C= -0.28 + 0.932.*Kt - 2.048.*(Kt.^2);
end
if(Kt>0.60)
A = -5.743 + 21.77.*Kt -27.49.*(Kt.^2) +11.56.*(Kt.^3);
B = 41.4 - 118.5.*Kt + 66.05.*(Kt.^2) +31.9.*(Kt.^3);
C = -47.01 + 184.2.*Kt - 222.*(Kt.^2) +73.81.*(Kt.^3);
end
delKn = A + B.*exp(C.*AM1);
Knc = 0.866 - 0.122.*AM1 + 0.0121.*(AM1.^2) - 0.000653.*(AM1.^3) +
0.000014.*(AM1.^4);
Kn = Knc - delKn;
DNI=Kn*I;
DNI(phi>87 | GHI<1 | DNI<0) = 0;
Ib=DNI*cosd(phi);
Idiff=GHI-Ib;
Ipoa=Ib+Idiff+0.2;
Ipoa3=Ib+(Idiff)+0.2;
Itr=Ipoa;
Itr1=Ipoa-(array1(191,131));

```

```

if GHI==0
    Itr1=0;
end
if Itr1<0
    Itr1=0;
end
load('CT.mat')
Tcell=CellT(HR1,1)+((48-20)/800)*Itr;
Tcell1=CellT(HR1,1)+((48-20)/800)*Itr1;
HR1=HR1+1;
Pdc=(Itr/1000)*250*(1+((-0.44)*(Tcell-25)));
Pdc1=(Itr1/1000)*250*(1+((-0.44)*(Tcell1-25)));
Pac=0.965*Pdc*0.1533;
Pac1=0.965*Pdc1*0.1533;
if Pac<0
    Pac=Pac*-1;
end
if Pac1<0
    Pac1=Pac1*-1;
end
if Pac>250
    Pac=245;
end
if Pac1>250
    Pac1=245;
end
dn(LT,1)=Itr;
gh(LT,1)=Itr1;
Ipoa1=Ipoa;
y4=0;
if da <= 31
    Month(1,1)=(Month(1,1)+Ipoa1);
    PDC(1,1)=PDC(1,1)+Pdc;
    PAC(1,1)=PAC(1,1)+Pac;
    Year(1,1)=Year(1,1)+y4;
    ATTE(1,1)=ATTE(1,1)+Pac1;
    JAN(1,1)=JANS(1,1)+Pac;

elseif da >=32 && da <=59
    Month(1,2) = (Month(1,2)+Ipoa1);
    PDC(1,2)=PDC(1,2)+Pdc;
    PAC(1,2)=PAC(1,2)+Pac;

```

```

Year(1,2)=Year(1,2)+y4;
ATTE(1,2)=ATTE(1,2)+Pac1;
elseif da >=60 && da <=90
Month(1,3) = (Month(1,3)+Ipoa1);
PDC(1,3)=PDC(1,3)+Pdc;
PAC(1,3)=PAC(1,3)+Pac;
Year(1,3)=Year(1,3)+y4;
ATTE(1,3)=ATTE(1,3)+Pac1;
elseif da >=91 && da <=120
Month(1,4) = (Month(1,4)+Ipoa1);
PDC(1,4)=PDC(1,4)+Pdc;
PAC(1,4)=PAC(1,4)+Pac;
Year(1,4)=Year(1,4)+y4;
ATTE(1,4)=ATTE(1,4)+Pac1;
elseif da >=121 && da <=151
Month(1,5) = (Month(1,5)+Ipoa1);
PDC(1,5)=PDC(1,5)+Pdc;
PAC(1,5)=PAC(1,5)+Pac;
Year(1,5)=Year(1,5)+y4;
ATTE(1,5)=ATTE(1,5)+Pac1;
elseif da >=152 && da <=181
Month(1,6) =(Month(1,6)+Ipoa1);
PDC(1,6)=PDC(1,6)+Pdc;
PAC(1,6)=PAC(1,6)+Pac;
Year(1,6)=Year(1,6)+y4;
ATTE(1,6)=ATTE(1,6)+Pac1;
elseif da >=182 && da<=212
Month(1,7) = (Month(1,7)+Ipoa1);
PDC(1,7)=PDC(1,7)+Pdc;
PAC(1,7)=PAC(1,7)+Pac;
Year(1,7)=Year(1,7)+y4;
ATTE(1,7)=ATTE(1,7)+Pac1;
elseif da >=213 && da <=243
Month(1,8) = (Month(1,8)+Ipoa1);
PDC(1,8)=PDC(1,8)+Pdc;
PAC(1,8)=PAC(1,8)+Pac;
Year(1,8)=Year(1,8)+y4;
ATTE(1,8)=ATTE(1,8)+Pac1;
elseif da >=244 && da <=273
Month(1,9) = (Month(1,9)+Ipoa1);
PDC(1,9)=PDC(1,9)+Pdc;
PAC(1,9)=PAC(1,9)+Pac;
Year(1,9)=Year(1,9)+y4;

```

```

        ATTE(1,9)=ATTE(1,9)+Pac1;
elseif da >=274 && da <=304
    Month(1,10) = (Month(1,10)+Ipoa1);
    PDC(1,10)=PDC(1,10)+Pdc;
    PAC(1,10)=PAC(1,10)+Pac;
    Year(1,10)=Year(1,10)+y4;
    ATTE(1,10)=ATTE(1,10)+Pac1;
elseif da >=305 && da <=334
    Month(1,11) =(Month(1,11)+Ipoa1);
    PDC(1,11)=PDC(1,11)+Pdc;
    PAC(1,11)=PAC(1,11)+Pac;
    Year(1,11)=Year(1,11)+y4;
    ATTE(1,11)=ATTE(1,11)+Pac1;
elseif da>=335 && da <=365
    Month(1,12) =(Month(1,12)+Ipoa1);
    PDC(1,12)=PDC(1,12)+Pdc;
    PAC(1,12)=PAC(1,12)+Pac;
    Year(1,12)=Year(1,12)+y4;
    ATTE(1,12)=ATTE(1,12)+Pac1;
    end
end

end

CD=ccdfplot(PAC);
set(gca,'YScale','log')
set(CD,'color','b');
set(CD,'linewidth',2);
hold on;
CD1=ccdfplot(ATTE);
set(gca,'YScale','log')
set(CD1,'color','m');
set(CD1,'linewidth',2);
hold on;

if da <= 31
    Month(1,1)=((Month(1,1)))/31;
    PDC(1,1)=PDC(1,1)/31;
    PAC(1,1)=PAC(1,1)/31;
    Year(1,1)=Year(1,1)/31;
    ATTE(1,1)=ATTE(1,1)/31;
elseif da >=32 && da <=59
    Month(1,2) = ((Month(1,2)))/28;
    PDC(1,2)=PDC(1,2)/28;

```

```

PAC(1,2)=PAC(1,2)/28;
Year(1,2)=Year(1,2)/28;
ATTE(1,2)=ATTE(1,2)/28;
elseif da >=60 && da <=90
    Month(1,3) = ((Month(1,3)))/31;
    PDC(1,3)=PDC(1,3)/31;
    PAC(1,3)=PAC(1,3)/31;
    Year(1,3)=Year(1,3)/31;
    ATTE(1,3)=ATTE(1,3)/31;
elseif da >=91 && da <=120
    Month(1,4) = ((Month(1,4)))/30;
    PDC(1,4)=PDC(1,4)/30;
    PAC(1,4)=PAC(1,4)/30;
    Year(1,4)=Year(1,4)/30;
    ATTE(1,4)=ATTE(1,4)/30;
elseif da >=121 && da <=151
    Month(1,5) = ((Month(1,5)))/31;
    PDC(1,5)=PDC(1,5)/31;
    PAC(1,5)=PAC(1,5)/31;
    Year(1,5)=Year(1,5)/31;
    ATTE(1,5)=ATTE(1,5)/31;
elseif da >=152 && da <=181
    Month(1,6) =((Month(1,6)))/30;
    PDC(1,6)=PDC(1,6)/30;
    PAC(1,6)=PAC(1,6)/30;
    Year(1,6)=Year(1,6)/30;
    ATTE(1,6)=ATTE(1,6)/30;
elseif da >=182 && da<=212
    Month(1,7) = (Month(1,7))/31;
    PDC(1,7)=PDC(1,7)/31;
    PAC(1,7)=PAC(1,7)/31;
    Year(1,7)=Year(1,7)/31;
    ATTE(1,7)=ATTE(1,7)/31;
elseif da >=213 && da <=243
    Month(1,8) = ((Month(1,8)))/31;
    PDC(1,8)=PDC(1,8)/31;
    PAC(1,8)=PAC(1,8)/31;
    Year(1,8)=Year(1,8)/31;
    ATTE(1,8)=ATTE(1,8)/31;
elseif da >=244 && da <=273
    Month(1,9) = ((Month(1,9)))/30;
    PDC(1,9)=PDC(1,9)/30;
    PAC(1,9)=PAC(1,9)/30;

```

```

    Year(1,9)=Year(1,9)/30;
    ATTE(1,9)=ATTE(1,9)/30;
elseif da >=274 && da <=304
    Month(1,10) = ((Month(1,10)))/31;
    PDC(1,10)=PDC(1,10)/31;
    PAC(1,10)=PAC(1,10)/31;
    Year(1,10)=Year(1,10)/31;
    ATTE(1,10)=ATTE(1,10)/31;
elseif da >=305 && da <=334
    Month(1,11) =((Month(1,11)))/30;
    PDC(1,11)=PDC(1,11)/30;
    PAC(1,11)=PAC(1,11)/30;
    Year(1,11)=Year(1,11)/30;
    ATTE(1,11)=ATTE(1,11)/30;
elseif da>=335 && da <=365
    Month(1,12) =((Month(1,12)))/31;
    PDC(1,12)=PDC(1,12)/31;
    PAC(1,12)=PAC(1,12)/31;
    Year(1,12)=Year(1,12)/31;
    ATTE(1,12)=ATTE(1,12)/31;
end

```

```

for da=1:365;
    NR=da*96;
    NR6=NR-95;
load('YE2015.mat')
y4=Y2015(NR6,1);
NR6=NR6+4
if da <= 31

```

```

    Year(1,1)=Year(1,1)+y4;
    MON(1,da)=MONS(1,1)+y4;
elseif da >=32 && da <=59

```

```

    Year(1,2)=Year(1,2)+y4;

```

```

elseif da >=60 && da <=90

```

```

    Year(1,3)=Year(1,3)+y4;

```

```

elseif da >=91 && da <=120

```

```

    Year(1,4)=Year(1,4)+y4;
elseif da >=121 && da <=151

    Year(1,5)=Year(1,5)+y4;
elseif da >=152 && da <=181

    Year(1,6)=Year(1,6)+y4;
elseif da >=182 && da<=212

    Year(1,7)=Year(1,7)+y4;
elseif da >=213 && da <=243
Year(1,8)=Year(1,8)+y4;
elseif da >=244 && da <=273

    Year(1,9)=Year(1,9)+y4;
elseif da >=274 && da <=304

    Year(1,10)=Year(1,10)+y4;
elseif da >=305 && da <=334

    Year(1,11)=Year(1,11)+y4;
elseif da>=335 && da <=365

    Year(1,12)=Year(1,12)+y4;
    end
end
if da <= 31

    Year(1,1)=Year(1,1)/31;
elseif da >=32 && da <=59

    Year(1,2)=Year(1,2)/28;

```

```
elseif da >=60 && da <=90
    Year(1,3)=Year(1,3)/31;
elseif da >=91 && da <=120
    Year(1,4)=Year(1,4)/30;
elseif da >=121 && da <=151
    Year(1,5)=Year(1,5)/31;
elseif da >=152 && da <=181
    Year(1,6)=Year(1,6)/30;
elseif da >=182 && da<=212
    Year(1,7)=Year(1,7)/31;
elseif da >=213 && da <=243
    Year(1,8)=Year(1,8)/31;
elseif da >=244 && da <=273
    Year(1,9)=Year(1,9)/30;
elseif da >=274 && da <=304
    Year(1,10)=Year(1,10)/31;
elseif da >=305 && da <=334
    Year(1,11)=Year(1,11)/30;
elseif da>=335 && da <=365
    Year(1,12)=Year(1,12)/31;
```

end


```
A=ccdf(CKY,1);
semilogy(A,'b','linewidth',1);
hold on;
C=ccdf(ATTE,1);
semilogy(C,'r','linewidth',1);
hold on;
B=ccdf(REAL,1);
semilogy(B,'g','linewidth',1 );
grid on;
ylabel('PROBABILITY');
legend('CLEAR SKY','ATTENUATION','REALTIME')
xlabel('OUTPUT POWER')
xlim([1,200]);
ylim([-3,1]);
```